5-1-2018

Stratigraphic Reconstruction of a Late Pleistocene Bald Cypress Forest Discovered on the Northern Gulf of Mexico Continental Shelf

Suyapa Michell Gonzalez Rodriguez
Louisiana State University and Agricultural and Mechanical College

STRATIGRAPHIC RECONSTRUCTION OF A LATE PLEISTOCENE BALD CYPRESS FOREST DISCOVERED ON THE NORTHERN GULF OF MEXICO CONTINENTAL SHELF

A Thesis

Submitted to the Graduate Faculty of the
Louisiana State University and
Agricultural and Mechanical College
In partial fulfillment of the
requirements for the degree of
Master of Science

in

The Department of Geology and Geophysics

by
Suyapa Michell Gonzalez Rodriguez
B.S. Louisiana State University, 2016
August 2018

Acknowledgements

I would like to first and foremost thank my thesis advisor and mentor, Dr. Sam Bentley, for giving me the opportunity to work on such an amazing project early in my career and for all his motivation. I owe my success as an undergraduate and graduate student to his dedication and all the guidance he has given me since the beginning. I am forever grateful for his trust and all his support. I would also like to thank the members of my thesis committee: Drs. Kehui Xu and Carol Wilson, for contributing tremendous amounts of knowledge to this project.

I would like to thank Dr. Kristine DeLong, from the Department of Geography and Anthropology at LSU, for all her input and knowledge she provided to this project, Dr. Jeff Obelcz for his help in collecting, processing and interpreting the geophysical data, and Jonathan Truong for his contributions in microfossil analysis and Petrel model. I also thank Dr. Zhixiong Shen of Coastal Carolina University for the OSL dating of our sediment samples. This project was made possible through the funding of BOEM (Bureau of Ocean Energy Management) award #M15AC00016.

I would also like to thank the CSI field work crew, including Chris Cleaver and Charlie Sibley, for their help in conducting the field work for this project, for their assistance with the core logger, and Rodney Stieffel, Brianna Crenshaw, Jeff Duxbury, Jonathan Camelo, Ryder Myers, and Samantha Hall for all their help in the field and sample preparation. I would like to thank Crawford White for teaching me how to use the GeoTek core logger.

Lastly, I would like to thank the most important people in my life, my parents and my brother, for their unconditional love, extensive support, and for always believing in me. This thesis is dedicated to them and to my beloved country, Honduras.

Table of Contents

List of Tables

List of Figures

Abstract

A previously buried bald cypress forest (*Taxodium distichum*) was discovered on the continental shelf, offshore of Orange Beach, Alabama, USA, in ~20 m water depth. The forest was exhumed by Hurricane Ivan in 2004, and is now exposed as stumps in life position in a trough located in the northern Gulf of Mexico continental shelf seafloor. We are investigating the local stratigraphy, paleo-landscape, and mode of forest preservation of this unique site. In August 2015 and July 2016, submersible vibracores (18 in total) were collected. Core analysis included: bulk density and imaging via Geotek multi sensor core logger, sediment grain size, structure, and organic content via loss-on-ignition. Selected samples have been dated using ^{14}C and optically stimulated luminescence (OSL) methods. Multibeam and CHIRP subbottom bathymetry provide context for litho- and chrono-stratigraphy of the site.

Integration of core lithostratigraphy and modern shelf bathymetry reveal Holocene transgressive sands blanketing diverse sedimentary facies that are truncated by the late Pleistocene-early Holocene ravinement. Deposits below the ravinement surface include a Holocene interbedded sand and mud, overlying a swamp facies of woody debris, peat, and mud (dated by OSL to 72±8 ka). These units grade laterally into paleosols that appear to be 10-16 ka younger, based on OSL dates. Occurrence of paleosols and swamp deposits of broadly similar age and elevation suggests that the ancient landscape possessed topographic relief that allowed wetland and upland habitats to develop in close proximity.

Floodplain aggradation in the area was a key factor that allowed forest preservation. Two temporary sea-level rises of 10-15 m occurred ca. 40 ka and another one of 30-35 m occurred ca. 60 ka, produced two pulses of local floodplain aggradation that buried the swamp and forest

sediments. During the subsequent lowstand, sediments that comprise the floodplain were eroded. Subsequently, paleosols were formed in nearby areas. Some swamp sediments located in paleo-topographic lows were preserved and buried due to the deep coverage of the eastern-trending channel infill sediments. Coastal wave erosion during transgression eroded high ground but enough sediment remained to keep the cypress forest blanketed and therefore allowed preservation until recent marine exposure.

Introduction

The Gulf of Mexico (GoM) is a complex and dynamic system that is governed by fresh water discharge (e.g., Morey et al., 2003), open ocean circulation (e.g., Hamilton, 1990), changes in sea level (e.g., Törnqvist et al., 2004), tropical storms (e.g., Stone et al., 2004; Reese et al., 2008), and subsidence in some locations (e.g., Jankowski et al., 2017; Törnqvist et al., 2008; Turner, 1991; Yu et al., 2012). Even though many studies have been conducted regarding the geologic setting and sea level variations in the area during the Holocene, relatively little is known about the late Pleistocene geology and stratigraphic architecture of the northeastern Gulf of Mexico, especially along the continental shelf south of Alabama. Moreover, Marine Isotope Stages (MIS) 3-5 are also not very well documented in the climatic record of the northern Gulf of Mexico. Paleoclimate reconstructions are essential to the understanding of the processes that drive changes in ancient climates and also greatly contribute to the prediction of future ones.

Previous studies (e.g., McBride and Byrnes, 1995; McBride et al., 1996; McBride et al., 1999; Bartek et al., 2004) have determined that the regional stratigraphy of the inner continental shelf south of Alabama, our study area, consists of: Holocene sands containing abundant shells, underlain by estuarine and other coastal deposits of Pleistocene to Holocene age.

_____

Some of the work of this thesis was previously published as: Gonzalez, S., S. J. Bentley, Sr., K. L. DeLong, K. Xu, J. Obelcz, J. Truong, G. L. Harley, C. A. Reese, and A. Caporaso, 2017, Facies reconstruction of a late Pleistocene cypress forest discovered on the northern Gulf of Mexico continental shelf: Gulf Coast Association of Geological Societies Transactions, v. 67, p. 133–146.
Is reprinted here by permission of Gulf Coast Association of Geological Societies

During the past decade, an example of copse tree stumps, mostly bald cypress trees (*Taxodium distichum*) in life position have been identified exposed on the continental shelf seabed, south of the Alabama shoreline (Gonzalez et al., 2017). Their water depth and location initially suggested their ages to be late Pleistocene to early Holocene.

The location of these well-preserved tree stumps is approximately 13 km offshore of Gulf Shores, Alabama at 18-20 meters below modern sea level (Fig. 1). This buried cypress forest can provide valuable insight into paleoenvironmental conditions, such as sea level variations, paleoclimate, and position of ancient shorelines of the region. The purpose of this proposed study is to investigate the depositional and stratigraphic setting of this ancient drowned forest, to better understand how such remarkable sedimentary deposits could be preserved at shallow depths on the continental margin through an entire glacial cycle.

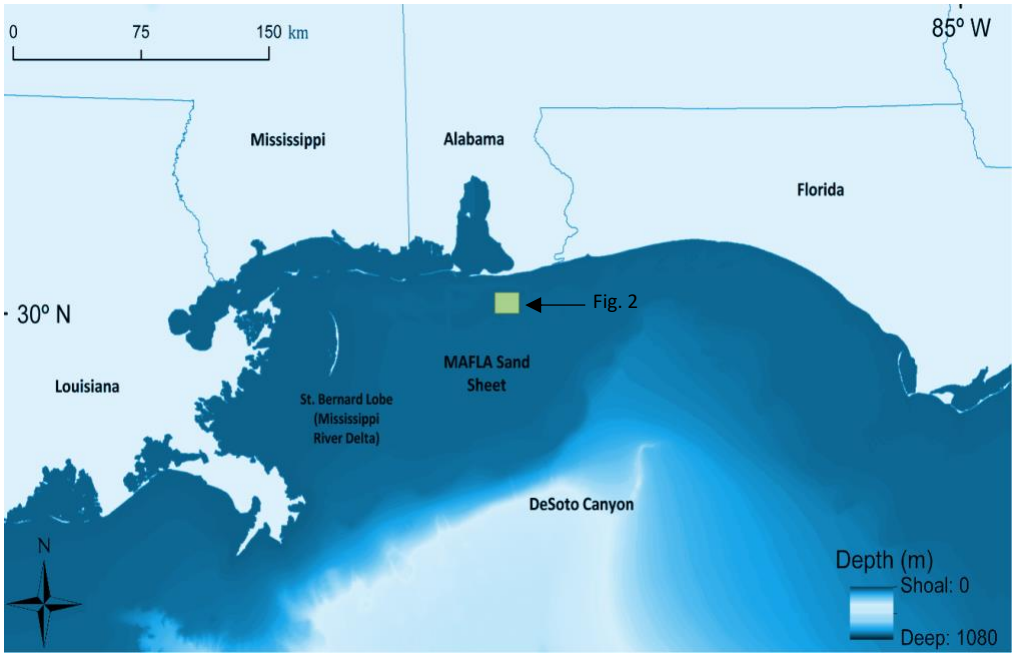

Figure 1. Basemap of study area showing approximate location of the ancient forest (green box) within the context of the northern Gulf of Mexico. Modified from Gonzalez et al., 2017.

Study Area

The study area of this project encompasses roughly 30,000 m^2 of the northern Gulf of Mexico continental shelf (Fig. 1). It is approximately 13 km south of Gulf Shores, Alabama. To the north, it is bounded by the Alabama shoreline, to the west by the St. Bernard Lobe of the Mississippi River Delta system, and to the southeast by the DeSoto Canyon. Water depths at the study sites for both surveys were about 18 to 20 meters below present day sea level. Low microtidal range and a low sediment-supply regime dominate this area (NOAA, Tides and Currents, 2013).

The cypress stumps of this study are currently exposed in a trough that is approximately 1.5 m deep below ambient sea floor. The seabed encompassing our study area is known as the MAFLA (Mississippi-Alabama-Florida) sand sheet, which is also subdivided into two subprovinces, the Mobile and the Apalachicola (Mazzulo and Peterson, 1989). A succession that fines upwards and horizontally westward is observed in the MAFLA sand sheet (McBride et. al., 1999). Furthermore, this sand sheet is made up of northwest-southeast trending ridges and troughs. From recent geophysical surveys and seafloor mapping, various locations of drowned cypress trees have been identified (Gonzalez et al., 2017; Obelcz, 2017; Ryu et al., 2016). Location of cores can be found on the bathymetric map (Fig. 2), which is identified in Figure 1.

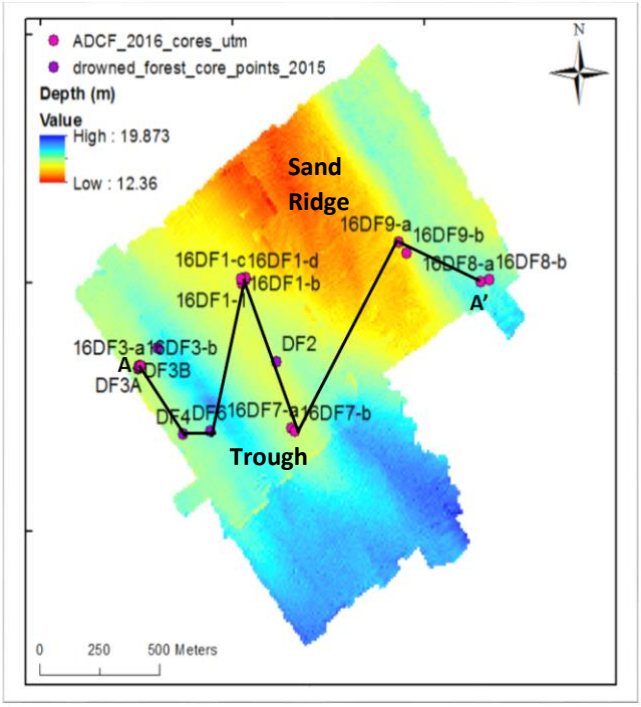

Figure 2. Bathymetric map of study site showing core locations from both field surveys. Warm colors indicate shallow bathymetry, while cool colors represent deeper bathymetry. A-A' cross section is shown on Figure 9. Modified from Obelcz, 2017.

Geologic Setting

The Gulf of Mexico during the Holocene

The Holocene is defined as an interglacial interval in the past roughly 12,000 years during which proxy-climate records are characterized as highly variable (Zoore et al., 2003). Although overall described as a warm period, Marine Isotope Stage (MIS) 1, the Holocene has experienced small scale oscillations in climate with notably warmer and cooler climate, such as the most recent cold event (the Little Ice Age) and the preceding Medieval Warm Period (Keigwin and Jones, 1989). Due to deglaciation and therefore presence of meltwaters in ocean water, sea level highstand dominates the Holocene and flooding of the continental shelf.

The GoM has been subject to progressive rise in sea level during the Holocene. Sea level rise at some locations in the northern GoM is directly associated with changes in global eustatic sea level (Donoghue, 2011). However in other places, like southern Louisiana, relative sea level is mostly controlled by local processes like subsidence due to sediment loading and compaction in the Mississippi River Delta (Törnqvist et al., 2004; Törnqvist et al., 2008). Changes in sea level consequently result in changes in shoreline position and therefore regional stratigraphy. Using relative sea level (RSL) curves, studies characterize Holocene sea-level changes as smooth RSL rise and others as a "step-stair" pattern (Törnqvist et al., 2004).

Tide-gauge records in the GoM show that for the past century sea level has risen about 2 mm/year. Late Pleistocene and early-middle Holocene rates were much higher, until near-present sea level was attained in the northern Gulf of Mexico about 6,000 years ago (Donoghue, 2011). Sea level rose rapidly from the Last Glacial Maximum, when global sea levels were as much as 125 meters lower than present, to present late Holocene levels, decelerating around 6,000 years

ago (Fig. 3) (Waelbroeck et al., 2002). The Last Glacial Maximum was encompassed by Marine Isotope State (MIS) 2 (29-14 ka), followed by MIS 1 for the Holocene (14-0 ka) (Lisiecki and Raymo, 2005). The Holocene slowdown in rate of sea level rise during this time period, MIS 2, allowed for the development of coastal land forms in the area. Since that time, shoreline position has been approximately stable (Donoghue, 2011).

Regional Geology

The most extensive surficial Pleistocene deposits of coastal origin consist of the Citronelle Formation, an extensive siliciclastic, deltaic deposit formation found across the Gulf Coastal Plain. The prominent lithology are comprised of unconsolidated, coarse-detrital sands. Clays, silts, and gravels are also observed in this formation and can be traced all the way from Florida to Texas (USGS, 2015; Isphording and Lamb, 1971). Pollen analysis dates this formation to the Late Pliocene (ca. 3.4-2.7 Ma) (Otvos, 1998), with other studies placing the youngest ages in early Pleistocene (Ipshording and Lamb, 1971). The Citronelle Formation's thickness is still uncertain due to overlying Pleistocene strata and erosion constantly occurring in the upper most section (Isphording and Lamb, 1971). In terms of depositional conditions, literature has placed the Citronelle Formation to be exclusively formed in fluvial settings (e.g. Matson 1916; Isphording and Lamb, 1971; Otvos, 1998).

Above the Citronelle Formation, less extensive Pleistocene deposits have not been studied in the same detail as the Citronelle, but have been mapped and described by Carlston (1950) and Otvos (1985), among others. The Late Pleistocene deposits on land closest to our study area are described by Carlston (1950) as being "marine, estuarine, and stream deposits of

Pamlico age," which conforms broadly with the MIS 5 highstand (Doar et al., 2014). (Fig. 3). Deposits studied in core, outcrop, and trenches include yellowish sand and clay, blue clay with rotten wood fragments, and lignitic beds that are generally similar to Pleistocene strata described by McBride et al. (1999) from the sub-Holocene strata of the MAFLA region, and also in this study.

Bald Cypress Trees

Bald cypress trees (*Taxodium distichum*) have long dominated the forests of wetland regions, especially the riverine and deltaic swamp forests along the Gulf Coast (Conner and Toliver, 1990; Wilhite and Toliver, 1990; Kennedy, 1972). They can be found in a wide range of climatic conditions, seasonally inundated plains where drainage occurs, and at elevations of up to several hundred meters above sea level, as long as inundation and climate conditions are right (Little, 1971; Wilhite and Toliver, 1990). Bald cypress trees thrive in subtropical environments, like the modern Gulf Coast region (Conner and Toliver, 1990). Additionally, cypress are able to withstand flooding and punctual or temporary amounts of salt intrusion (Hook, 1984). However, they are not found in brackish or saline waters. Like any other type of wetlands in the region, bald cypress forests are also subject to the effects of regional sea level rise and increase in flooding and salinity. The environments in which bald cypress trees are found are mainly associated with seasonal inundation (Conner and Day, 1988). Furthermore, such species has been widely used for climate reconstruction by using dendrochronology (Keim and Amos, 2012). More information on the hydrological regime of the area can be obtained from wetland tree dendrochronology (Keim and Amos, 2012).

Based on the preferred habitats for bald cypress (freshwater coastal/flood plains with seasonal inundation), approximate time frames can be identified when the forest may have grown, by studying the sea-level curves like the one in Figure 3. The bathymetric depth range of our study site, 18-20 meters below sea level (mbsl), intersects sea level near times of ~10,000 ka, 80,000 ka, 110,000 ka, 118,000 ka and 125,000 ka. Therefore, the time between about 10,000 ka and about 125,000 ka thus represents a possible time interval during which this forest may have grown.

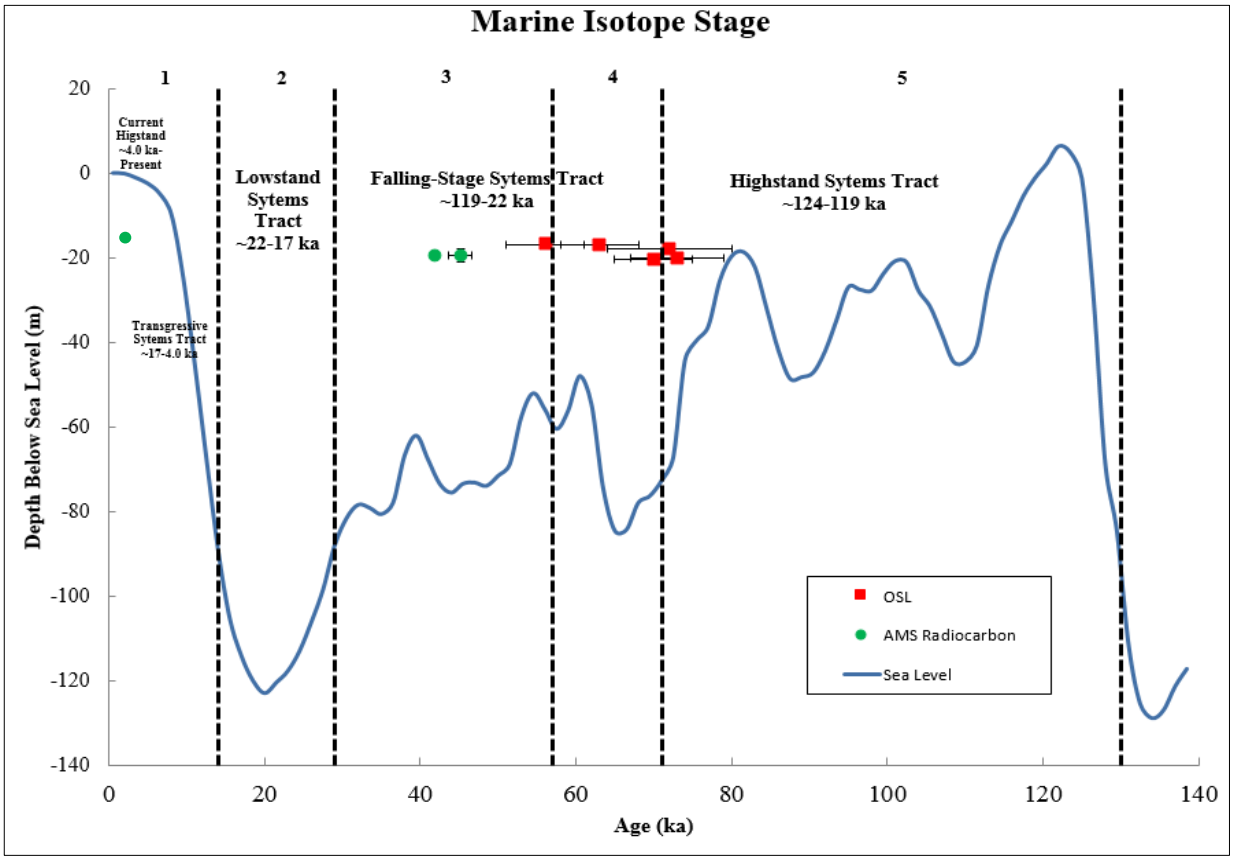

Figure 3. Relative sea level curve of the past 140,000 ka. ^{14}C dates from core DF-1 (green) and OSL dates from cores 16 DF-3A, 16 DF-7A. 16 DF-7B, 16 DF-8A, and 16 DF-9A (red) are shown. Their respective horizontal error bars are also shown. Sea level data from Waelbroeck et al. (2002).

Objectives

- Document and characterize the sediments that buried and preserved the cypress trees. A detailed description of the different sedimentary facies found in the study site will provide better insight to how, when, and why the tree stumps were preserved.
- Establish an absolute geochronology for forest growth and burial. This is a key factor for reconstructing the geologic and depositional history of the area
- Identify sediment ages and the extent of the Holocene-Pleistocene unconformity in vibracores using OSL and ^{14}C dates and microfossil work from companion study.
- Recognition and interpretation of the sedimentary facies preserved at the site will lead to a broader understanding of environmental and ecosystem changes in this region of the northern Gulf of Mexico margin in the late Pleistocene and early Holocene time. This time frame is not well documented in the region, because many of the sedimentary records have been eroded and in many cases drowned from rising sea level during the Holocene.

Methods

Field Work and Data Collection

Vibracoring

Eighteen vibracores were collected offshore of Gulf Shores, Alabama in the study area in August 2015 and July 2016 onboard the *R/V Coastal Profiler* of Louisiana State University's Coastal Studies Institute at water depths of about 18-20 mbsl. A submersible vibracorer with a 6 m long, 7.5 cm diameter aluminum casing was used to collect cores up to 5 meters long (Fig. 4). In August 2015, ~17.08 m of cores were collected and in July 2016 ~26.16 m. After recovery, cores were cut into 1.5 m sections. Sediment trapped in core catchers was stored in Whirl Pak bags and retained for foraminifera analysis. Cores were stored in refrigeration room located in the Geology Department at LSU.

Geophysical Data

Geophysical data were collected by Drs. Kehui Xu and Jeffrey Obelcz from the Department of Oceanography and Coastal Sciences at LSU. Swath bathymetry, chirp sub-bottom, and sidescan sonar data were collected during both surveys (Obelcz et al., 2014; Obelcz, 2017). Geophysical instruments used in both surveys (2015 and 2016) are: EdgeTech 2000 combined dual frequency side scan sonar and sub-bottom profiler on the starboard side, EdgeTech 512i sub-bottom profiler on the port side, EdgeTech 4600 swath bathymetry and side scan sonar on the bow. Wide bandwidth, tight line spacing, slow boat speed, and a high ping rate were used to maximize horizontal resolution of the trough. Data collection and processing

methods are described in Obelcz et al. (2014). Geophysical data were used for this project to better understand regional bathymetry, but those data are not the focus of this thesis.

Figure 4. Vibracoring tripod used to collect sediment cores of up to 5 m in length. Image by Kristine DeLong.

Data Processing and Analysis

Gamma Density

Soon after core collection, cores from the 2015 and 2016 surveys were logged using a Geotek Multi-Sensor Core Logger (MSCL) for whole-core gamma density of sediments. Cores DF-1, DF-2, DF-3A, DF-3B, DF-4, DF-5, and DF-6 from the 2015 field work and cores 16 DF-1C, 16 DF-3B, 16 DF- 8B, and 16 DF-9B from the 2016 field work were analyzed for density profiles.

All cores were split in half longitudinally. Each section was placed inside plastic tubes for safe storage, one archive half for future studies and one working half for the current project.

All cores were stored in a 4°C cold room. The working half of each core collected was sub-sampled for granolumetric and organic-content analyses. Samples for grain size and organics were taken at an interval of 2 cm. A high resolution image for the archive half each core was generated using a Geotek MSCL-XZ digital imaging system.

Grain Size

Core sub-samples underwent grain size analysis on a Beckman Coulter LS 13-320 Laser-Diffraction Particle Analyzer. First, each sediment sub-sample was wet sieved at 850 μm in order to get rid of any particles too large for the instrument or any organic debris. Sub-samples were then submerged in a 0.05% sodium meta phosphate solution and vortexed to deffloculate particles. H_2O_2 was then added to this aliquot to remove any remaining organic matter. Samples were placed in a hot bath at 70°C overnight to further deflocculate the particles. Finally, samples were transferred into 40 mL test tubes and capped with sodium meta phosphate before undergoing grain size analysis. Data is presented as frequency plots (Fig. 5 and Appendix A.2) and mean grain size (Fig. 6 and Appendix A.3)

LOI and Organic Content

Organic content analysis was conducted using the LOI (loss on ignition) technique (Heiri et al., 1999). Sub-samples were taken every 2 cm. The samples were weighed and put in an oven for 72 hours at a temperature of 60 °C. Dry mass was then measured after dehydration to assess water content and porosity. Next, sub-samples were put in a furnace for 2 hours at 550 °C. Finally, the samples were weighed again to measure loss on ignition and percent organic matter.

Radiocarbon Dating

^{14}C dating methods were used to obtain absolute dates for the Pleistocene sediments and bald cypress trees found in the study site. Seven sub-samples from core DF-1 were taken at the following depths: 3.22 m (from an interbedded sand and mud layer), 4.05 m, 4.19 m, 4.24 m, 4.56 m, 4.07 m and two samples at 4.14 m (all from an organic-rich, peat-bearing sediments) (Fig. 9). A mixed benthic foram assemblage from core DF-1 at the 330 cm mark was also dated using this method (Troung et al., 2017) (Fig. 9). All samples were sent to Beta Analytic Radiocarbon Dating Laboratory for dating (Table 1).

Eleven wood samples previously collected, some in October 2013, by scuba divers, and others collected by Ben Raines from the Weeks Bay Foundation were sent to the Center for Accelerator Mass Spectrometry at the Lawrence Livermore National Laboratory in California, for additional ^{14}C dates. No ages were obtained from these samples (Table A.1, Appendix 1).

OSL Dating

Sub-sections of cores 16 DF-3A, 16 DF-7A, 16 DF-7B, 16 DF-8A, and 16 DF-9A were dated using OSL (optically stimulated luminescence) dating techniques. Dr. Zhixiong Shen from Coastal Carolina University sub-sampled the five cores on November, 2016. Each sample was selected based on the deepest portion of each core where coarse sediments that overlaid the swamp facies were located. Analysis used a silt sized fraction for dating (Shen et al., 2007; Shen and Mauz, 2012). Water content in all five samples contained approximately 20-28%, with core 16 DF-3A having the highest water content due to the presence of organics.

OSL results are presented in Table 2. Samples were underneath 20 meters of water (which was approximately the water depth of our study site) for ~15% of their burial time and sub-aerially exposed for the remainder. Results have an uncertainty of timing due to the changing of water content during the burial period and other associated analytical errors.

Results

Radiocarbon Dating

The initial dates for ^{14}C obtained from the sub-sample found in coarsely fibrous peat in core DF-1 at 414 cm depth revealed a radiocarbon age of 37.35 ± 0.33 ka (41.83 cal ka with a range of 42.23 to 41.35 cal ka at 95% probability, where cal ka is thousands of calendar years before 1950 Common Era) (Table 1; Fig 9). Calibrated age was determined using INTCAL13 (Reimer et al., 2013) following the parameters of Talma and Vogel (1993). Six of the other seven samples sent to Beta Analytic, came back as radiocarbon 'dead' (Table 1). The sample at 405 cm depth in DF-1, which is located at the boundary between interbedded peat and mud and overlying interbedded mud and sand (described below; Fig. 9), had a radiocarbon age of 41.83 ± 0.88 ka, and median calibrated age of 45.21 cal ka, and 95% probability range of 46.69–43.62 cal ka). This sample is older than the deeper 414 cm peat sample. The age result from the mixed benthic foram assemblage from core DF-1 located at 330 cm depth was 3940 ± 30 BP with a 95.4% probability (4045-3830 cal BP).

Because the radiocarbon ages from woody material are near the upper limit of reliable detection (ca. 40 ka), other cores from the site were dated with alternate absolute dating methods, such as optical stimulated luminescence (OSL). This additional dating extended the possible age range of the sediments in this study from the ^{14}C results. With this caveat, we used these dates cautiously for a preliminary core chronostratigraphy.

Table 1. Radiocarbon dates for sediment samples and a mixed benthic foram taken from core DF-1. Results were obtained from Beta Analytic Radiocarbon Dating Laboratory in Miami, Florida.

DF-1 Sediment Samples Radiocarbon Results						
Sample Type	**Sample Depth**	**$\delta^{13}C$**	**^{14}C age**	**±**	**Cal BP age**	**Cal BP range**
Plant material	322 cm	–30.1	>43500			
Plant material	405 cm	–28.8	41830	880	45210	46690–43625
Plant material	414 cm	–23.0	37350	330	41830	42235–41350
Plant material	414 (2) cm	–28.9	>43500			
Plant material	419 cm	–28.7	>43500			
Plant material	424 cm	–31.0	>43500			
Plant material	456 cm	–27.4	>43500			
Plant material	466 cm	–28.5	>43500			
Mixed Benthic Foram	330 cm			30	3940	4045-3830

OSL Dating

Optical stimulated luminescence (OSL) provided chronology control in addition to the previously obtained ^{14}C dates. OSL dates revealed sediments as old as 73±6 ka from core 16 DF-7A and sediments as young as 56±5 ka from core 16 DF-8A (Fig. 3). Results from all five cores analyzed for OSL dating are given in Table 2 below.

Table 2. OSL dates for sediment samples obtained from five distinct cores. Facies dated is indicated by colors. Data from Dr. Zhixiong Shen at Coastal Carolina University.

Sample Name	Water/Sample Depth (m)	$^{238}U \pm 1\sigma$ (µg g-1)	$^{232}Th \pm 1\sigma$ (µg g-1)	$K_2O \pm 1\sigma$ (µg g-1)	Water Content (%)	OSL age ±1σ (ka)
16 DF-3A	15.8/2.12	2.96±0.09	11.61±0.34	1.37±0.04	0.57±0.10	**72±8**
16 DF-9A	14.4/2.57	4.18±0.11	12.43±0.27	1.33±0.03	0.25±0.10	**63±5**
16 DF-7B	15.7/4.58	3.50±0.10	12.01±0.28	1.16±0.03	0.24±0.10	74±6 61±7
DF 7B-1 Weighted Mean						**70±5**
16 DF-7A	15.7/4.30	3.52±0.09	12.63±0.28	1.34±0.03	0.27±0.10	**73±6**
16 DF-8A	16.2/0.60	4.96±0.13	17.02±0.35	1.52±0.04	0.20±0.10	**56±5**

Interbedded Sand and Mud
Interbedded Mud and Peat
Paleosol

Physical Properties of Sediments

Grain size frequency contour plots were generated using the results obtained from the laser-diffraction analysis. Distinct grain size changes and distribution can be observed down section in each core (Fig. 5; Appendix A.2). The upper most section of each core is noted as sand-sized sediments with a high percent volume, >5%. Depending on the core, the interbedded sand and mud are also observed in these frequency plots (~300-405 cm from DF-1; ~60-296 cm from DF-3B in Fig. 5). Furthermore, this is consistent with the varying gamma density readings for this interval. The same concept applies to the interbedded mud and peat and paleosol sediments. For these units,

frequency plots tend to show a 2-4% modal grain size found within the clay and silt division in the graph (Fig. 5; Appendix A.2).

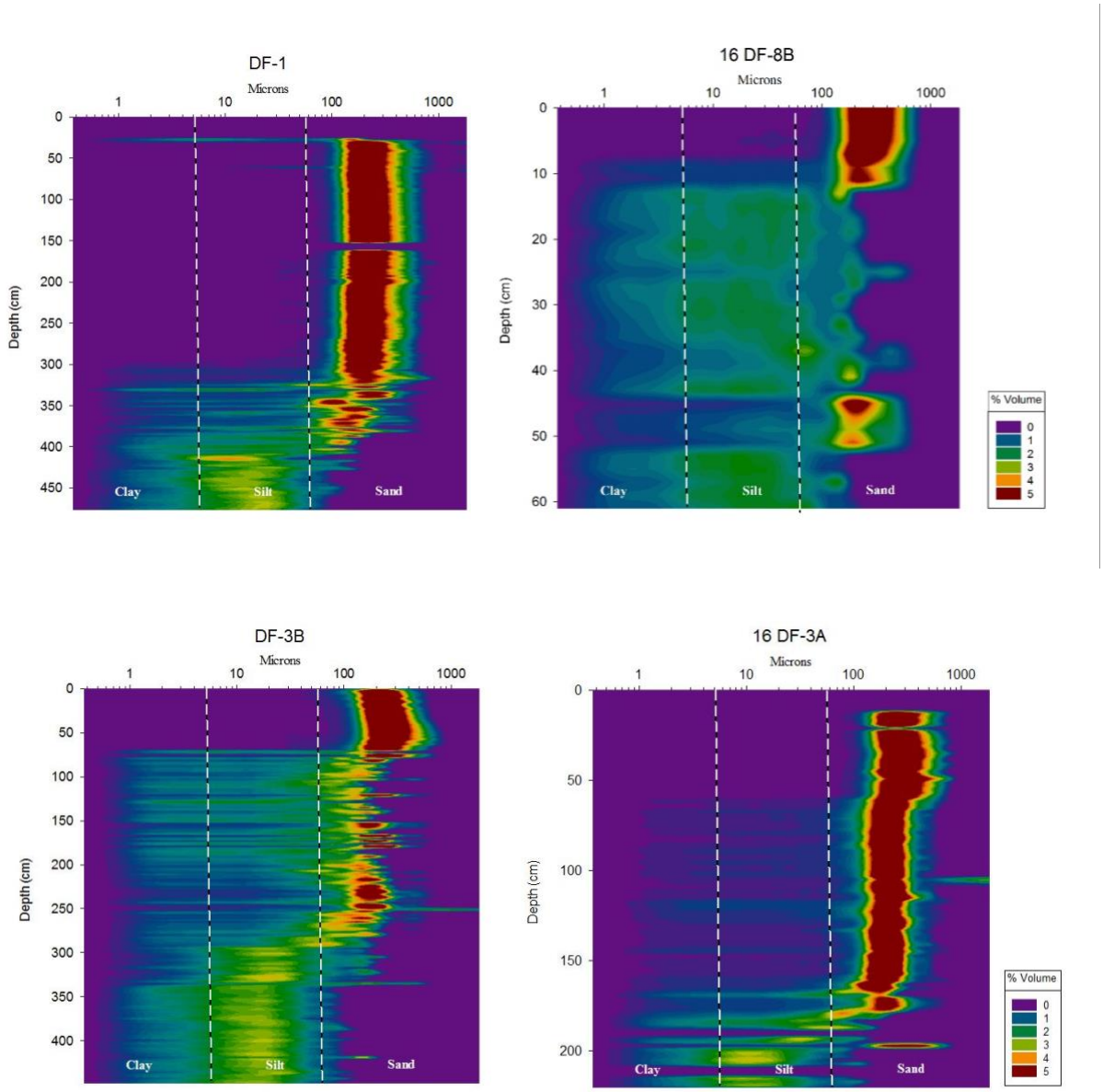

Figure 5. Selected frequency contour plots for grain size distributions. Core grain size is shown as a color contour plot of % volume versus depth. Warm colors indicate dominant grain size for that depth in microns. Other frequency plots can be found in Appendix B.

Gamma density profiles revealed distinctive variations in sediment density versus depth within each lithological unit found in the cores that were analyzed (Fig. 6; Appendix A.3). The top most lithological unit displayed high density readings, which was identified as a sandy unit. Density readings range from ~2.3 g/cm^3 to ~2.5 g/cm^3. The next underlying unit was identified as interbedded sand and mud sediments (Fig. 6; Appendix A.3). Density readings here were generally high and widely variable, ~1.8-2.3 g/cm^3 (310-405 cm on core DF-1 from Fig. 6). Following this unit, are interbedded muds and peats sediments. This unit displayed low and variable densities, 1.2-1.9 g/cm^3 (405-478 on core DF-1 from Fig. 6). The last lithological unit was identified as a paleosol, which showed gamma density readings of 1.9-2.4 g/cm^3 (~10-60 cm on core 16 DF-8B from Fig. 6). Overall, the gamma density of sediments in each core decreases down section. Some sandy sections were found to have settled during storage, causing erroneous density readings. These sections are labeled as "disturbed core" in each core density profile (Fig. 6).

Loss on ignition (LOI) results helped determine the organic content in sediment cores. Throughout Figures 6 and A.3, variability in organic content can be observed down section (green triangles). In each core, the uppermost sandy unit contained roughly up to 1% in organic content (OC). A slight increase in OC is noted in the interbedded sand and mud unit: ~1.3-2.6%. As for the interbedded mud and peat unit, OC was as high as ~20.3%. The paleosol found only in cores 16 DF-8A and 16 DF-8B displayed low organic content, 0.6-3.8%.

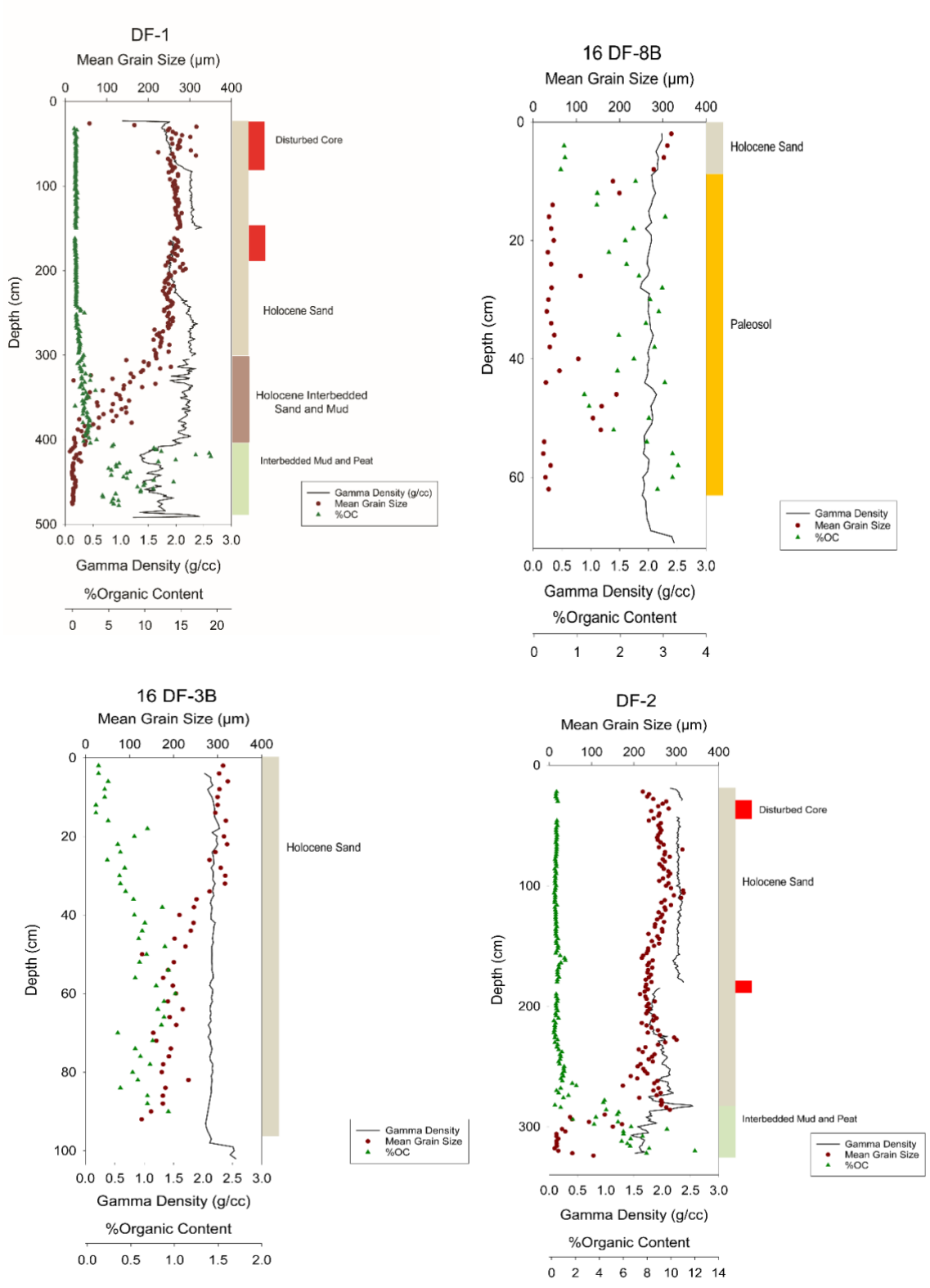

Figure 6. Selected comprehensive graphs from cores collected in 2015 and 2016 showing gamma density, grain size, and organic content. Other comprehensive graphs are in Appendix C.

Geophysical Data

From geophysical data (swath bathymetry, CHIRP sub-bottom, and sidescan sonar), geological 3D model that integrates core data and geophysical data was created using Petrel suite (Fig. 7). This model displays 3 surfaces. The uppermost is bathymetry (study site seafloor) and the two underlying surfaces were identified as transgressive ravinement surface and bay head delta/fluvial surface (Obelcz, 2017). Each core is georeferenced to its respective depth and location and is "hanging" from the seafloor. This model aided in understanding the regional geology and locating subsurface contacts. Regional bathymetry revealed the extent of a seafloor trough that was previously identified in a survey conducted by investigators from the University of Southern Mississippi in 2012. Bathymetry revealed a system of northwest-southeast trending ridges and troughs. This was remapped at greater extend and resolution by Obelcz (2017).

The surficial sand sheet (MAFLA Sand Sheet of McBride et al., 1999) is thickest at the ridges (0-5 m) and thinnest or absent inside the trough located in our study site (Fig. 2 and Fig. 7). The cypress stumps are exposed in the trough. The bathymetric surface converges with the ravinement surface in the deepest part of the trough located in the study area (Fig. 7). Accommodation space and paleotopography is observed between the ravinement and basal surface where the preserved forest is found (Fig. 7). The interpretation for the bottom-most surface in this model, bay head/fluvial surface, is based on seismic data and line picks from Obelcz (2017). Unfortunately, our cores did not penetrate deeply enough to sample these strata. Therefore, there is no sedimentary evidence that can corroborate this interpretation.

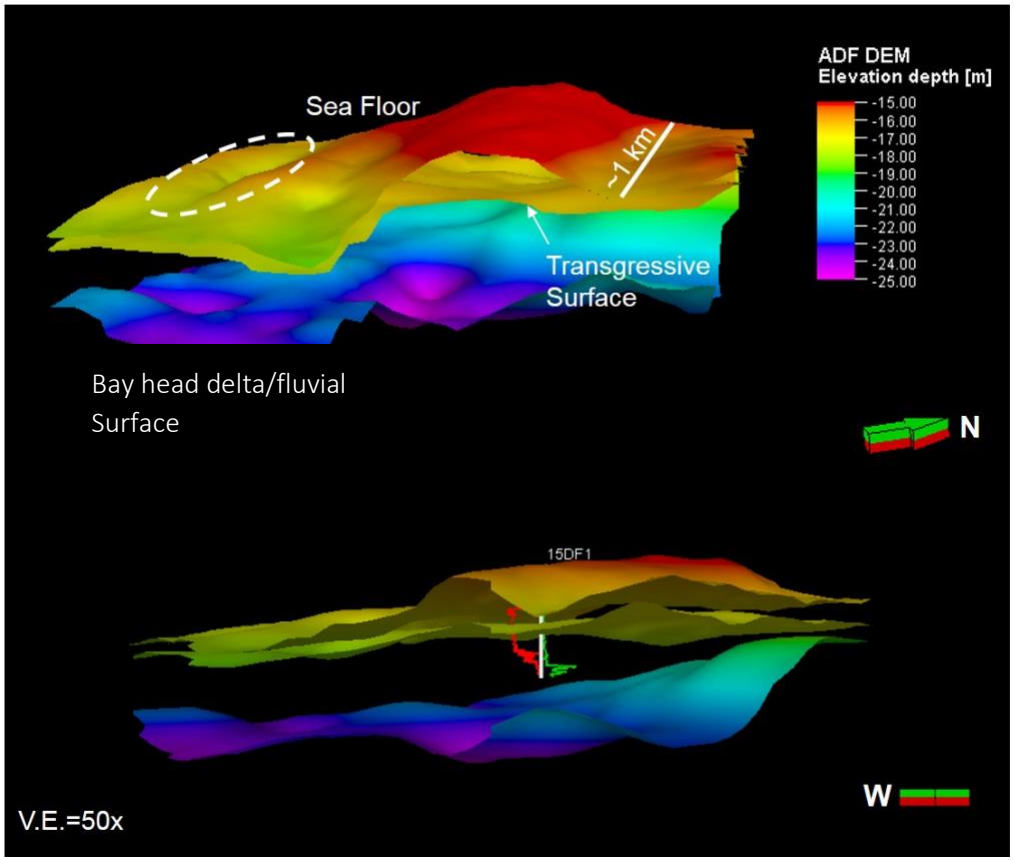

Figure 7. Geological 3D model showing study site seafloor underlain by a transgressive surface and a third surface interpreted as a bay head delta/fluvial (Obelcz, 2017).

Facies Interpretation

Lithofacies and Age

Based on gamma density, grain size, organic content, and sediment observations, five different lithologic units (facies) characterize the sedimentary deposits found in the study area. From the gamma-density profiles of sediment cores (Fig. 5), higher density readings are associated with larger grain sizes and lower porosity, like those in sand-sized sediments. In contrast, lower density readings correlate to smaller grain sizes and higher porosity found in sediments like clays, silts, and zones of high organics. As for organic content, shelf sands, like those found at our study site, tend to have little to no organic content. In contrast, swampy and tree stump-bearing sediments exhibit a much higher organic content. These trends can be observed in the comprehensive plots on Figure 5.

Facies descriptions presented below are derived from core DF-1 (Gonzalez et al., 2017). Facies descriptions from Gonzalez et al. (2017) were applied to comparable lithologic units in the other 17 cores. Two new facies classifications were developed. The fourth and fifth facies, named a Pleistocene interbedded sand and mud and a Late Pleistocene paleosol, were found only in five cores: 16 DF-8A and 16 DF-8B 9 for the paleosol facies and 16 DF-7A, 16 DF-7B, and 16 DF-9A for the Late Pleistocene interbedded sand and mud facies (Fig. 6; Table 3; Appendix A.3). Four of the facies (facies 1, 2, 3, and 5 below) are consistent with the lithologic descriptions of McBride et al. (1999). Facies descriptions below are from the top to the bottom of core DF-1 (Gonzalez et al., 2017) except facies 4 (Pleistocene interbedded sand and mud) and facies 5 (paleosol). Facies characteristics were consistent in all of the cores (Fig. 8; Table 3). Lithofacies names are generally considered to be age-independent (North American Commission

on Stratigraphic Nomenclature, 2005), and we follow that practice here. However, in order to provide more concise and effective litho- and chrono-stratigraphic descriptions, age and facies of strata identified in vibracores are described together below. Facies depth ranges are different for each core.

Facies 1: Holocene Sand

Facies 1 (0-310 cm) is characterized by light, beige to grey, fine- to medium-grained quartz sand containing abundant bioclasts and shell fragments (Figs. 8-9). Color becomes progressively lighter up section, with some intervals slightly darker than others. Sediments are moderately to well sorted. Minor planar bedding is present. The foraminiferal assemblage found in the top 310 cm is consistent with a shallow marine environment. Most of the bioclasts found are highly fragmented and vary in size. A prominent shell bed of 5-15 cm thick is also found within this facies in some cores. This facies is consistent with facies 5 and 6 from McBride et al. (1999) described in that study as primarily sand, and shelly sand. These sand sheet deposits are thickest on the ridges and thinnest or completely absent in the troughs of the study site (Fig. 6). This facies is present on all cores of the study (Fig. 6 and Table 3).

Facies 2: Holocene Interbedded Sand and Mud

Facies 2 (310-405 cm) is characterized by light to medium dark grey mud interbedded with very fine grained sub-bioclastic sand, and to some extent shell fragments (Figs. 8-9). Fine-grained sand occurs in beds that are well sorted and have no sedimentary structures present other than prominent sand-mud interbedding. Beds are mostly 1–3 cm thick. In some intervals, mud is

more abundant than sand. This unit is present in these cores: DF-1, DF-3B, DF-4, and 16 DF-3A, (Table 3).

Evaluation of microfossils suggests a shallow marine assemblage with a radiocarbon age of 4045-3830 cal BP taken at the 330 cm mark of core DF-1 (Truong et al., 2017). Gulf of Mexico sea level curves from the Holocene puts this ^{14}C date at roughly 3 m below present day sea level (Fig. 3) (Donoghue, 2011). This interpretation, combined with OSL ages (72±8 ka) for the underlying unit, indicates that an unconformity exists between facies 2 and facies 3. We hypothesize the location of the erosional unconformity is somewhere between the 330 cm and 405 cm mark on core DF-1. Furthermore, this same unconformity should be present in other cores that exhibit a similar stratigraphy. However, the exact location of this unconformity in sediment cores is not clear with this dataset. Therefore, possible differences between Gulf of Mexico sea levels and the Waelbroeck et al. (2002) global sea level record must be considered.

Facies 3: Late Pleistocene Interbedded Mud and Peat

This facies (405–478 cm) is characterized by dark grey, tan to dark brown muds and peats. Some intervals are darker than others, especially those where wood debris is found (Figs. 8-9). Organic material and wood debris are abundant. Wood fragments are light brown in color and roughly 1–2 cm thick. No sedimentary bed forms are present, but bedding is clear in alternating peat and mud layers. Wood debris visible in core correlate stratigraphically to the bald cypress stumps exposed in the scoured basin evident on Figures 6 and 7. This is also the facies sampled for ^{14}C dating on core DF-1 and for OSL dating on core 16 DF-3A. This facies was not identified by McBride et al. (1999), but is present in several cores of our study area:

DF-1, DF-2, DF-3B, DF-4, DF-4, DF-5, DF-6, 16 DF- 1D, and 16 DF-3A (Fig. 6; Table 3; Appendix A.3).

Macro and microfossils are absent in the samples studied, but pollen analysis from companion study (Reese et al., 2018, in review) showed an assemblage that is consistent with a bald cypress-tupelo gum forest for the last portion of this facies in core DF-1 (445-475 cm on Fig. 9) (Reese et al., 2017 in review). This assemblage changes between 435-450 cm where percentages of cypress and tupelo gum pollen decline sharply and are replaced by grass and sedge pollen. This change is likely associated with a more open, possibly brackish environment as sea levels increased during the transition out of MIS 3. However, from 430-420 cm in the core, the percentages of cypress increase again, and are codominant with alder (*Alnus*).

Initially, ^{14}C ages of this unit from core DF-1 ranged from ~41,000 to >50,000 yr (i.e., radiocarbon dead, Table 1), suggesting an approximate time of MIS 3 or older (Fig. 3). OSL results from a comparable interbedded mud and peat found in core 16 DF-3A, later dated this unit to be 72 +/- 8 ka, placing it near the boundary between MIS 4 and 5 (Fig. 3). Sediment properties of this unit are consistent with deposition in a bald cypress swamp (producing peat and woody debris) in a river floodplain (providing mud beds from episodic flooding) (Smith and Bentley, 2014; Heitmuller et al., 2017). Overall, there is a coarsening upwards sequence in core DF-1, where all three facies (Holocene sand, Holocene interbedded sand and mud, and Late Pleistocene interbedded mud and peat) are bioturbated to some extent (Fig. 9) (Gonzalez et al., 2017).

Facies 4: Late Pleistocene Interbedded Sand and Mud

This facies displays similar grain size to Facies 2 (Holocene interbedded sand and mud), although fine sand has a more dominant %volume (4-5%) in this facies and there is a 100-180 μm mean grain size compare to Facies 2 (110-200 μm) (Fig. 8; Appendix A.2-3). However, the depositional environment is different for both. Facies 2 was produced by a marine setting. This assumption is supported by a radiocarbon date of 4045-3830 cal BP and the presence of marine benthic foraminifera within the unit. OSL dates from cores 16 DF-7A, 16 DF-7B, and 16 DF-9A range from 63-73 ka (Table 2). This clearly indicates that such facies is Pleistocene in age and we infer from the Waelbroeck et al. (2002) sea level curve that it must be terrestrial in terms of depositional environment. 80 ka is approximately the earliest time (before the Holocene) in which such interbedded sand and mud would have been deposited by marine conditions at this depth (18-20 mbsl). This leads us to conclude that this facies was deposited by a terrestrial, fresh water system during the late MIS 5 and early MIS 4. Such stratigraphy of interbedded sand and mud produced by a terrestrial, fluvial source has been observed in other parts of the Gulf Coast, such as in the Atchafalaya Basin in Louisiana (Roberts, 1997).

Facies 5: Late Pleistocene Paleosol

This last facies is characterized by light grey, yellowish, and orange colored silt and clay sized sediments and is only present in two cores: 16 DF-8A and 16 DF-8B (Figs. 6; 8; Table 3; Appendix A.3). This unit was identified by McBride et al. (1999) as their Facies 1. Evidence of near subaerial exposure is confirmed by the clear traces of oxidation found in these sediments. Organic content readings were low. On core 16 DF-8A the paleosol is ~70 cm thick and on core

16 DF-8B the thickness is ~50 cm. The OSL age obtained from core 16 DF-8A is 56 +/- 5 ka (Table 2), which places this paleosol in the late Pleistocene. Such a relatively young age compared to the other cores dated for OSL, suggests that the location of this core must have been on an area with high relief and exposure. Furthermore, age constraints from this facies and the overlying Holocene sand indicate the presence of an erosional unconformity between these deposits (McBride et al., 1999). No macro or microfossils are present in this facies.

Table 3. Facies location and depths for sediment cores used in this study. "L. Pleist" = Late Pleistocene.

Core ID	Interval (cm)	Facies
DF-1	0-310	Holocene Sand
	310-405	Holocene Interbedded Sand and Mud
	405-478	L.Pleist. Interbedded Mud and Peat
DF-2	0-275	Holocene Sand
	275-330	L. Pleist. Interbedded Mud and Peat
DF-3A	0-106	Holocene Sand
DF-3B	0-60	Holocene Sand
	60-296	Holocene Interbedded Sand and Mud
	296-453	L. Pleist. Interbedded Mud and Peat
DF-4	0-120	Holocene Sand
	120-167	Holocene Interbedded Sand and Mud
	167-194	L. Pleist. Interbedded Mud and Peat
DF-5	0-14	Holocene Sand
	14-112	L. Pleist. Interbedded Mud and Peat
DF-6	0-47	Holocene Sand
	47-93	L. Pleist. Interbedded Mud and Peat

(table cont'd.)

Core ID	Interval (cm)	Facies
16 DF-1B	0-94	Holocene Sand
16 DF-1C	0-166	Holocene Sand
16 DF-1D	0-364	Holocene Sand
	364-392	L. Pleist. Interbedded Mud and Peat
16 DF-3A	0-62	Holocene Sand
	62-177	Holocene Interbedded Sand and Mud
	177-220	L. Pleist. Interbedded Mud and Peat
16 DF-3B	0-96	Holocene Sand
Core ID	**Interval (cm)**	**Facies**
16 DF-7A	0-100	no sediments
	100-150	Holocene Sand
	150-193	no sediments
	193-300	Holocene Sand
	300-370	no sediments
	370-405	Holocene Sand
	405-464	L. Pleist. Interbedded Sand and Mud
16 DF-7B	0-206	Holocene Sand
	206-444	L. Pleist. Interbedded Sand and Mud
16 DF-8A	0-10	Holocene Sand
	10-80	L. Pleist. Paleosol
16 DF-8B	0-10	Holocene Sand
	10-62	L. Pleist. Paleosol
16 DF-9A	0-186	Holocene Sand
	186-267	L. Pleist. Interbedded Sand and Mud
16 DF-9B	0-175	Holocene Sand
	175-230	L. Pleist. Interbedded Sand and Mud

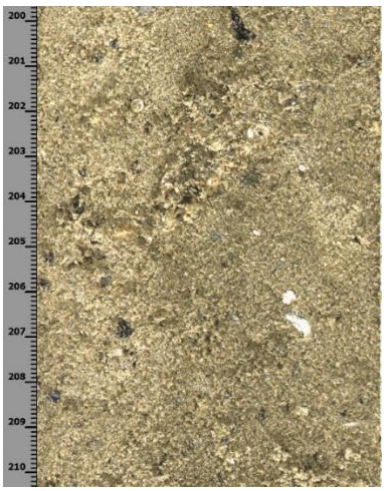

Facies 1: Holocene Sand

Facies 2: Holocene Interbedded Sand and Mud

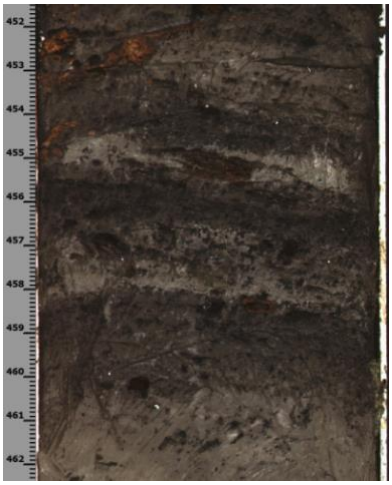

Facies 3: Late Pleistocene Interbedded Mud and Peat

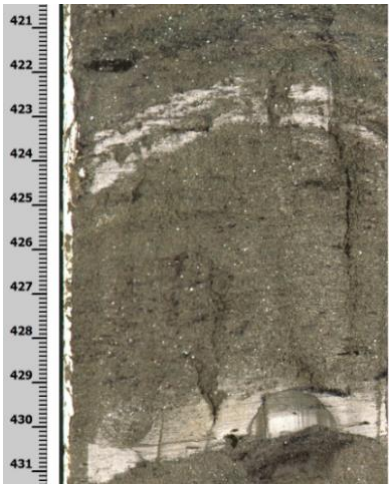

Facies 4: Late Pleistocene Interbedded Sand and Mud

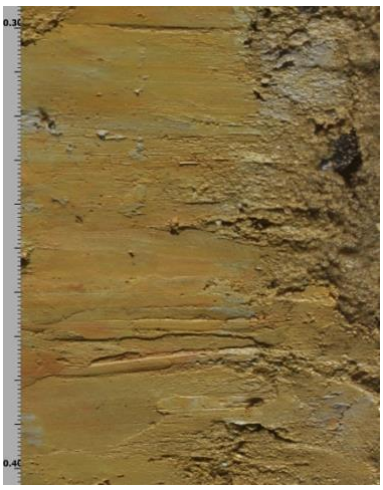

Facies 5: Late Pleistocene Paleosol

Figure 8. High-resolution imagery of the five lithofacies found in the study cores. See Table 3 for facies interval.

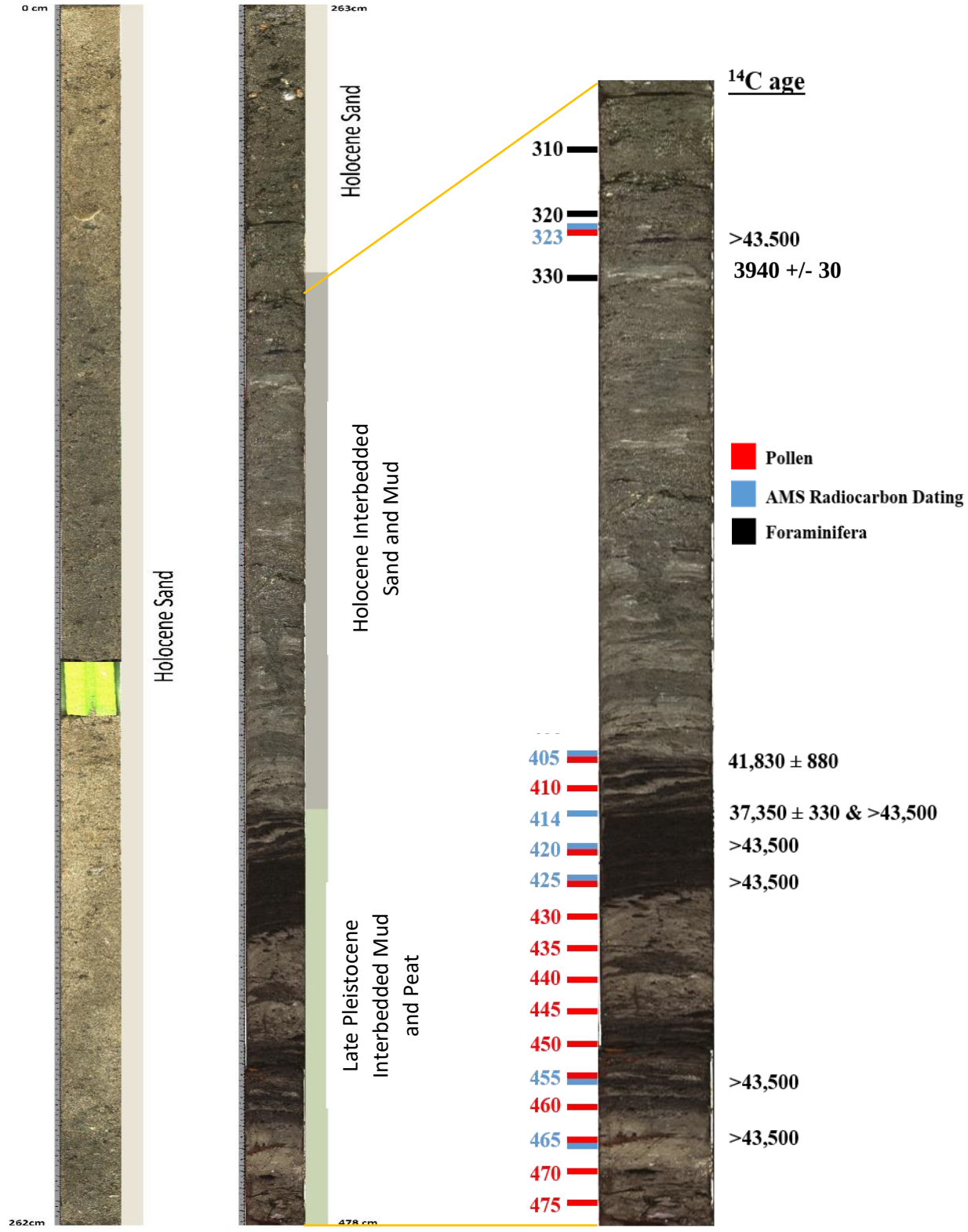

Figure 9. Left: High-resolution imagery of core DF-1 showing facies. Right: Pollen (Reese et al., 2018, in review) and radiocarbon sample locations in core DF-1 (Table 1).

Discussion

Regional Stratigraphy

The depositional environments and regional stratigraphy of the study area during the Pleistocene and the Holocene have been greatly impacted by changes in sea level in the northern Gulf of Mexico. Consequently, events of marine transgression and regression have played a major role in shaping the stratigraphy observed at this site today.

From all 18 sediment cores, five different lithofacies were identified, although no core contained all five lithofacies (Fig. 8). These are: a Holocene sand sheet; a Holocene interbedded sand and mud (shallow marine); a Late Pleistocene interbedded sand and mud, a Late Pleistocene paleosol, and a Late Pleistocene interbedded mud and peat unit, potentially from an ancient river floodplain (this assessment is also supported by preliminary analysis of seismic data; Obelcz, 2017) (Fig. 6; Table 3; Appendix A.3). Consistency was found among some of these facies and those described by McBride et al. (1999). However, identification of Pleistocene river-swamp deposits appears to be unique to this study. The Late Pleistocene interbedded sand and mud, and late Pleistocene paleosol are broadly consistent with the geology of the Citronelle Formation and overlying sedimentary strata of MIS 5/Pamlico age exposed on the nearby coastal plain (Carlston, 1950; Isphording and Lamb, 1971; Otvos, 1985; USGS, 2015; Otvos, 1998). The base of cores DF-1, DF-2, DF-3B, DF-4, DF-5, DF-6, 16 DF-1D, and 16 DF-3A stratigraphically correlate with the cypress stump-bearing horizon (Fig. 6; Table 3; Appendix A.3).

An East-West cross section across the trough and ridge shows the stratigraphy in our study area (Fig. 10). From depth at which the cores were collected, we are able to observe variability in elevation of facies contacts. This variability in facies, which likely reflects

paleotopographic relief, is a key factor for forest preservation that allowed for an accommodation space to be created and therefore deep burial of the forest to happen.

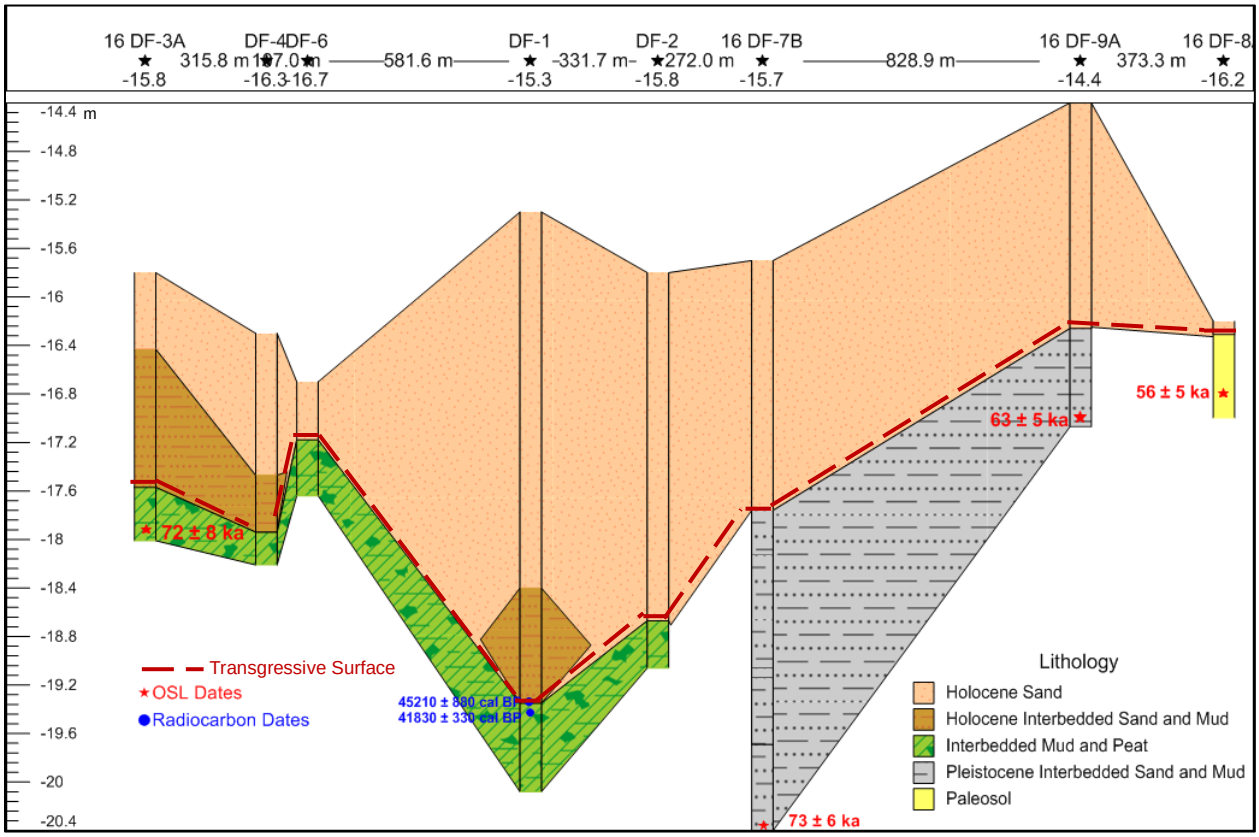

Figure 10. Stratigraphic cross section A-A' (Fig. 2) and map from across the study site. Correlation of facies can be observed with all five units. OSL and ^{14}C dates are also plotted at their respective depths. Cores are georeferenced to their respective depths and locations.

By integrating stratigraphy and age models, it is plausible to conclude that some areas were buried before others. For example, the bottom of the Pleistocene interbedded sand and mud on core 16 DF-7B has an age of 73 -/+ 6 ka and it is the deepest core in our study site, in terms of absolute elevation (Fig. 10). In contrast, the bottom of core 16 DF-8A has the youngest age of 56 +/- 5 ka and it is the shallowest core. Therefore, older ages are stratigraphically and topographically located below younger ages. This finding is confirmed by the presence of highly oxidized paleosols found in two cores (16 DF-8A and 8B), which indicate that the

paleotopographic highs in the study site were subaerially exposed on the continental shelf prior to the Holocene Transgression that further eroded and flooded the area (Figs. 3; 10).

Effects of Sea Level Change & Flood Plain Aggradation on Forest Preservation

This unique scenario in which bald cypress trees and enclosing river-swamp deposits have been preserved for likely over 70,000 yrs is a geological puzzle. Age (see OSL results on Table 2) and depth relationships (Figs. 3; 10) cannot with certainty explain how the cypress forest could withstand periods of erosion during the late Pleistocene sea level fall and Holocene sea level rise. Sea level around 70 ka was in the range of -20 to -90 m below present sea level (Fig. 3), and regional topographic relief was relatively low. One interpretation of these observations is that the swamp developed at an elevation above and possibly distant from sea level and the shore.

To develop a more detailed interpretation, we assume that the ages of dated sediments (via ^{14}C and OSL) are all reliable, that actual ages are near the median age estimates for each sample (Figure 3; Tables 1 and 2), and that the global sea level curve of Waelbroeck et al. (2002) applies to the Gulf of Mexico shoreline with negligible correction required for glacioisostacy or other factors, considering the relevant timescales and spatial scales, For example, during MIS 3 and 4, eustatic rapid sea level rises and falls of >10 m occurred over periods of <5,000 years (Fig. 3).

These deposits were buried and protected from erosion during a period of up to 70,000 yrs of regression, transgression, and extensive subaerial exposure during the Last Glacial Maximum. For this to happen, these deposits were originally buried by a substantial (and

unknown) thickness of sediments, which were mostly but not entirely eroded during Pleistocene exposure and Holocene transgression. Absolute age results and core lithology indicate that the stratigraphic record of tens of thousands of years from the area was eroded away (Fig. 10).

One potential process that could have produced abundant sediment burial is floodplain aggradation. Two temporary sea-level rises of 10-15 m occurred ca. 40 ka and another one of 30-35 m occurred ca. 60 ka (Fig. 3), produced two pulses of local floodplain aggradation that buried the swamp and forest sediments. Such rapid aggradation has been observed many kilometers inland in other coastal-plain alluvial valleys, where rivers aggrade rapidly in order to "keep up" with pulses in sea level rise (Anderson et al., 2016; Shen et al., 2012, 2015). During MIS 5, there was an aggradation event along the Gulf Coast (Shen et al., 2015). Anderson et al. (2016) also observed congruent floodplain aggradation to rise in local sea level for small-to medium-sized rivers along the northwestern Gulf Coast in Texas during the late Quaternary (MIS 5-3).

From sea level curves like the one on Figure 3, it can be observed that fluctuations in sea level occurred during MIS 5- 3. Events of valley aggradation could have occurred in our study area in a similar fashion that they occurred in the region surveyed by Anderson et al. (2016), where sediment supply to marine basins was modulated by episodic changes in sea level. In contrast, their study also suggests that delta progradation can occur during low stands as sediment gets delivered to basins and back-stepping of deltas occurs (Fig. 11). While aggradation is favored during rising seas, valley incision can happen during the falling stages where sediment delivery is not as prominent (Blum et al., 2013).

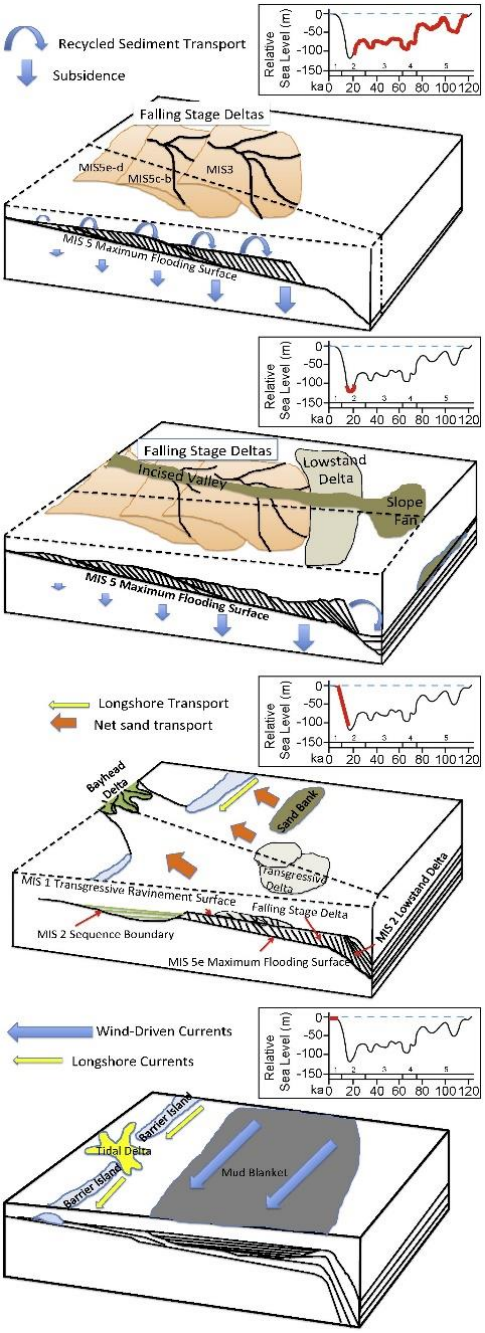

Falling Stage

1. Delta growth marked by episodic progradation and back-stepping due to sea-level oscillations
2. Recycling of sediments from the slowly subsiding inner shelf to the outer shelf results in increased sediment supply through time
3. Multiple episodes of channel incision and purging during fall and aggradation during rise contributes to variable sediment supply to deltas

Lowstand

1. Valley incision
2. Lowstand delta and slope fan formation
3. Continued erosion and recycling of sediments from inner to outer shelf

Transgression

1. Transgressive ravinement provides sand to evolving coast
2. Transgressive deltas formed during climatically-induced increase in sediment discharge of Brazos, Colorado, and Rio Grande rivers
3. Sand Banks formed by overstepping of barriers
4. Valley aggradation

Highstand

1. Most modern barriers formed
2. Sediment bypass in larger rivers
3. Mud blanket formed on central Texas shelf

Figure 11. Geologic events associated with the Falling Stage, Lowstand, Transgression, and Highstand Systems Tracts with their corresponding sea level curve. (From Anderson et al., 2016)

We hypothesize that the same phenomenon that produced floodplain aggradation during MIS 5 also occurred shortly after pulses of sea level rise in MIS 3-4, where the breaching of natural river levees can be caused by the overbank of sediment in the floodplain consistent with both the peat and mud facies and Pleistocene sand and mud facies. During lowstands, sea level falls and the sediments that comprise the floodplain are eroded. Subsequently, paleosols form in other nearby areas, as documented by McBride et al. (1999) as a basal facies in some of their cores and also in two cores (16 DF-8A and 8B).

Integration of published sea level curves (e.g. Waelbroeck et al., 2002), ^{14}C and OSL sediment ages, lithology, paleomorphology, and paleotopography suggest that forest preservation could have been accomplished by multiple phases of aggradation, and less likely, by falling-stage delta progradation, in concordance with the geological model of Anderson et al. (2016) developed for river systems of the northwestern Gulf of Mexico coastal plain. Anderson et al. (2016) documented periods of Late Pleistocene floodplain aggradation at rates equivalent to the rates of contemporaneous sea level rise pulses. In our case, we observe clustered sediment ages at or just before sea level rise pulses ca. 60 ka, 54 ka, and 40 ka (Fig. 3; Tables 1-2). These are preceded by dated sediments suggesting burial and aggradation between age of sediments and age of sea level peak.

In a third case, we find clustered OSL ages at the start of a relatively short period of sea level fall (late MIS 5 - early MIS 4), which was followed by another pulse of sea level rise ca. 60 ka (Fig. 3). In this case, floodplain aggradation due sea level rise soon after the dated sediments were deposited is not a plausible explanation. If the sediment ages are correct and immediate sediment burial did occur, then another mechanism needs to be invoked other than immediate response to sea level rise. The apparent elevation of the location above sea level ca. 60 ka (well

below the elevation of our study area at that time: Figure 3) suggests that delta progradation is not a likely explanation. However, if the actual record of GoM sea level rise differs from that of Waelbroeck et al. (2002), then aggradation and progradation scenarios proposed by Anderson et al. (2016) could be plausible for the preservation of sediments by burial ca. 70 ka.

The results presented here are at the northern limit of the area surveyed by Bartek et al. (2004). Bifurcation of the Mobile-Tensaw River system during the MIS 2 resulted in two incised valleys being re-occupied south of Mobile Bay (Fig. 12). One eastern-trending incised valley and one western-trending incised valley were identified by Bartek et al. (2004). The present site is located near the area encompassed by the eastern incised valley (red box on Figure 11). Sea level rise patterns in the area during the Holocene are interpreted to have led to transgression of the depositional environments associated with the incised valleys, therefore changing the position of the coastline. Figure 12 shows the approximate location of our study site near the eastern trending incised valley from the Bartek et al. (2004) study.

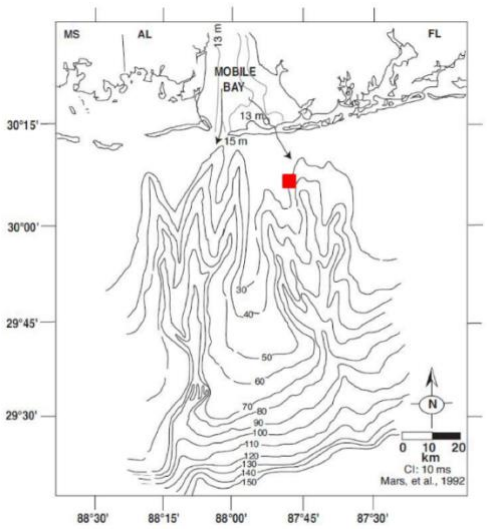

Figure 12. Time structure map of MIS (Marine Isotope Stage) 2 sequence boundary showing the two incised valleys located south of the modern Alabama shoreline. Contour interval is 10 ms. Modern shelf break is found at the 120 m contour. Redbox shows approximate location of study site. Modified from Bartek et al. (2004).

We propose that swamp sediments found in cores DF-1, DF-2, DF-3B, DF-4, DF-4, DF-5, DF-6, 16 DF- 1D, and 16 DF-3A, located in topographic lows were preserved and buried by fluvial/floodplain sediment accumulation. Finally, as sea level rose and transgression occurred during the late Plesitocene, sediments within the incised valleys were first eroded by transgression of the coastline and associated wave energy and later covered by Holocene shelf sands as sea level rose, thus causing the coastline position to retreat. Coastal wave erosion during transgression likely eroded high ground but enough sediment remained to keep the cypress forest blanketed, therefore fortuitously favoring preservation.

Another key component of this hypothesis, is that some accommodation space had to exist in order for thick packages of sediments to be deposited and therefore allow forest preservation. We support this assumption with our integrative DEM and the two underlying surfaces (Fig. 7). On Figure 7, an accommodation surface is being created by the bottom surface dipping southwest.

Conclusions

This unique scenario where cypress trees have been preserved for possibly over 70,000 yrs represents a puzzling geologic setting. Relatively rapid and deep burial by flood plain aggradation prevented exposure by channel incision and coastal erosion during the latest Pleistocene regression and Pleistocene-Holocene transgression, thus preserving the tree stumps and wood debris.

If this hypothesis is ultimately proven correct by further study, this could help identify the locations of other similar drowned forests of similar age around the Gulf of Mexico, because the depth range of such forest preservation would be caused by the regional impact of sea-level rise and associated flood plain transgression, similar to our study area, forming a sort of 'bathtub ring' around the Gulf of Mexico at common age and depth. These sites should be concentrated offshore of modern river systems that would have incised the shelf at lower sea levels and deposited sediments during the phase of flood plain aggradation around 70 ka ago that likely preserved our drowned forest. If hypothesis is correct, then each time there is pulse in sea level rise there should be a backwater effect and floodplain aggradation event that occurs in response to that rise in sea level.

References

Aitken, M.J., 1998, An introduction to optical dating: The dating of Quaternary sediments by the use of photon-stimulated luminescence: Oxford University Press, v. 267

Bartek, L.R., B.S. Carbote, T. Young, and W. Schroeder, 2004, Sequence stratigraphy of a continental margin subjected to low-energy and low-sediment-supply environmental boundary conditions; late Pleistocene-Holocene deposition offshore Alabama, U.S.A.: Late Quaternary Stratigraphic Evolution of the Northern Gulf of Mexico Margin, Special Publication, SEPM Society for Sedimentary Geology, no. 79, p. 85-109.

Bentley, S.J., T.R. Keen, C.A. Blain, and W.C. Vaughan, 2002, The origin and preservation of a major hurricane event bed in the Northern Gulf of Mexico: Hurricane Camille, 1969: Marine Geology, v. 186, p. 426-446.

Blum, M. J. Martin, K. Milliken, and M. Garvin, 2013, Paleovalley systems: insights from Quaternary analogs and experiments: Earth-Sci. Rev, v. 116, p. 128–169.

Carlston, C.W., 1950, Pleistocene history of coastal Alabama: Geological Society of America Bulletin, v. 61(10), p.1119-1130.

Conner, W.H., and J.W. Day, 1988, Rising water levels in coastal Louisiana — implications for 2 coastal forested wetland areas in Louisiana: J. Coast. Res, v. 4, p. 589–596.

Conner, W.J., and J.R. Toliver, 1990, Long Term Trends in the Bald-cypress (*Taxodium distichum*) resource in Louisiana (U.S.A.): Forest Ecology and Management, v. 33/34, p. 543-557.

Doar III, W.R. and C.G.S.C. Kendall, 2014, An analysis and comparison of observed Pleistocene South Carolina (USA) shoreline elevations with predicted elevations derived from Marine Oxygen Isotope Stages: Quaternary Research, v. 82(1), p.164-174.

Donoghue, J. F., 2011, Sea level history of the Northern Gulf of Mexico coast and sea level Rise scenarios for the near future: Climatic Change, v. 107, p. 17-33.

Gonzalez, Suyapa., Samuel J. Bentley Sr., Kristine L. DeLong, Kehui Xu, Jeffrey Obelcz, Jonathan Truong, Grant L. Harley, Carl A. Reese, Alicia Caporaso. 2017, Facies reconstruction of a Late Pleistocene cypress forest discovered on the Northern Gulf of Mexico Continental Shelf: Gulf Coast Association of Geological Societies Transactions, v. 67, p. 133-146.

Gonzalez, S., S.J. Bentley, K. DeLong, K. Xu, G.L. Harley, C.A. Reese, J. Obelcz, and J. Ryu, 2016, Geologic setting and preservation of a Late Pleistocene bald cypress forest discovered on the Northern Gulf of Mexico continental shelf: Ocean Sciences Meeting, New Orleans, LA.

Hamilton, P., 1990. Deep currents in the Gulf of Mexico: Journal of Physical Oceanography, v. 20(7), p. 1087-1104.

Heiri, O., A. F. Lotter, and G. Lemcke, 2001, Loss on ignition as a method for estimating organic and carbonate content in sediments: reproducibility and comparability of results: Journal of Paleolimnology, v. 25, p.101-110.

Heitmuller, F.T., P.F. Hudson, and R.H. Kesel, 2017. Overbank sedimentation from the historic AD 2011 flood along the Lower Mississippi River, USA: Geology, v. 45(2), p. 107-110.

Hook, D.D., 1984, Waterlogging tolerance to lowland tree species of the south: South Journal of Applied Forestry, v. 8(3), p. 136-149.

Jankowski, K L., T.E. Tornqvist, and A.M. Fernandez, 2017, Vulnerability of Louisiana's coastal wetlands to present-day rates of relative sea-level rise: Nature Communications, v. 8

Keen, T.R., S.J. Bentley, W. C. Vaughan, and C.A. Blain, 2004, The generation and preservation of multiple hurricane beds in the Northern Gulf of Mexico: Marine Geology, v. 210, p. 79-105.

Keim, R. F. and J. B. Amos, 2012, Dendrochronological analysis of baldcypress (Taxodium distichum) responses to climate and contrasting flood regimes: Canadian Journal of Forest Research, v. 42 (3), p. 423–436.

Keigwin, L.D., and G.A. Jones, 1989, Glacial-Holocene stratigraphy, chronology, and paleoceanographic observations on some North Atlantic sediment drifts: Deep Sea Research Part A. Oceanographic Research Papers, v. 36.6, p. 845-867.

Kennedy, H. E., Jr., 1972, Baldcypress: U.S Department of Agriculture Forest Service FS-218
Lisiecki, L.E., and M.E. Raymo, 2005, A Pliocene-Pleistocene stack of 57 globally distributed benthic 18O records: Paleoceanography, v. 20, PA1003

Little, E. L., Jr., 1971, Atlas of United States trees, volume 1, conifers and important hardwoods: U.S. Department of Agriculture Miscellaneous Publication, v. 1146: 9, p. 200 maps

Love, M.R., C.J. Amante, B.W. Eakins, and L.A. Taylor, 2012, Digital elevation models of the Northern Gulf Coast: procedures, data sources and analysis: NOAA Technical Memorandum NESDIS NGDC-59

Matson, G. C, 1919, The Pliocene Citronelle Formation of the Gulf Coastal Plain: US Government Printing Office, no. 98-L

Mazzullo, J., and M. Peterson, 1989, Sources and dispersal of Late Quaternary silt on the Northern Gulf of Mexico continental shelf: Marine Geology, v. 86, p. 15-26.

McBride, R.A., L.C. Anderson, A. Tudoran, and H.H. Roberts, 1999, Holocene stratigraphic architecture of a sand-rich shelf and the origin of linear shoals: northeastern Gulf of Mexico: SEPM Special Publications, v. 64, p. 95-126

McBride, R. A. and M. R. Byrnes, 1995, Surficial sediments and morphology of the southwestern Alabama western Florida Pan handle coast and shelf: Gulf Coast Association of Geological Societies Transactions, v. 45, p. 392-404

McBride, R. A., M.R. Byrnes, L.C. Anderson, and B.K. Sen Gupta, 1996, Holocene and Late Pleistocene sedimentary facies of a sand rich continental shelf: a standard section for the northeastern Gulf of Mexico: Gulf Coast Association of Geological Societies Transactions, v. 46, p. 287-299.

Morey, S.L., P.J. Martin, J.J. O'Brien, A.A. Wallcraft, and J. Zavala-Hidalgo, 2003, Export pathways for river discharged fresh water in the northern Gulf of Mexico: Journal of Geophysical Research, Oceans, 108(C10).

NOAA. "Sea Level Trends." NOAA Tides and Currents. NOAA10, 15 Oct. 2013.

North American Commission on Stratigraphic Nomenclature, 2005. North American stratigraphic code. *AAPG Bulletin*, *89*(11), pp.1547-1591.

Obelcz, J., 2017, Shallow stratigraphic and surficial analysis of a well-preserved Pleistocene drowned forest: how does it fit into the Northern Gulf of Mexico geologic context and how was it preserved?: Louisiana State University, Ph.D. dissertation

Obelcz, J., B. J. Brothers, U.T. Chaytor, S.W. Brink, S.W. Ross, and S. Brooke, 2014, Geomorphic characterization of four shelf-sourced submarine canyons along the U.S. Mid-Atlantic continental margin: Deep-Sea Research II, v. 104, p.106-119.

Otvos, E. G., 1998, Citronelle Formation, northeast Gulf Coastal Plain: stratigraphic and age issues: Gulf Coast Association of Geological Societies Transactions, v. 48, p. 321–333.

Otvos, E.G., 1985, Coastal Evolution-Louisiana to Northwest Florida: New Orleans Geological Society Guidebook, v. March 27-29, p. I-91.

Reese, C.A., T. P. Strange, W.D. Lynch, and K. Liu, 2008, Geologic evidence of Hurricane Katrina recovered from the Pearl River marsh, MS/LA: Journal of Coastal Research, p.1601-1607.

Reese, C. A., G.L. Harley, K. DeLong, S.J. Bentley, K. Xu, J.T. Truong, S. Gonzalez, J. Obelcz, A. Caparaso, 2018, Palynology of an autochthonous cypress forest of Late Pleistocene (MIS 3) age preserved on the northern Gulf of Mexico continental shelf, USA: Palaeogeography, Palaeoclimatology, Palaeoecology, in review

Reimer, P.J., E. Bard, A. Bayliss, J.W. Beck, P.G. Blackwell, C. Bronk Ramsey, C.E. Buck, H. Cheng, R.L. Edwards, M. Friedrich, P.M. Grootes, T.P. Guilderson, H. Haflidason, I. Hajdas, C. Hatté, T.J. Heaton, D.L. Hoffmann, A.G. Hogg, K.A. Hughen, K. F. Kaiser, B. Kromer, S.W. Manning, M. Niu, R.W. Reimer, D.A. Richards, E.M. Scott, J.R. Southon, R.A. Staff, C.S.M. Turney, J. van der Plicht, J, 2013, IntCal13 and

marine13 radiocarbon age calibration curves 0–50,000 years cal BP: Radiocarbon, v. 55, p. 1869-1887.
Roberts, H., N. Walker, R. Cunningham, G. Kemp, and S. Majersky, 1997, Evolution of sedimentary architecture and surface morphology: Atchafalaya and Wax Lake Deltas, Louisiana (1973–1994): Gulf Coast Ass. Geol. Soc. Trans, v. 47, p. 477–484.

Ryu, J., K. DeLong, S.J. Bentley, K. Xu, G.L. Harley, C.A. Reese, J. Obelcz, T. Guilderson, 2016, New evidence on an ancient bald cypress forest on the inner shelf of Northern Gulf of Mexico: Ocean Sciences Meeting, New Orleans, LA.

Shen, Z., T. E. Tornqvist, W. J. Autin, Z. R. P. Mateo, K. M. Straub, and B. Mauz, B, 2012, Rapid and widespread response of the Lower Mississippi River to eustatic forcing during the last glacial-interglacial cycle: Geological Society of America Bulletin, v. 124, p. 690–704.

Shen, Z., T. E. Törnqvist, B. Mauz, E. L. Chamberlain, A. G. Nijhuis, and L. Sandoval, 2015, Episodic overbank deposition as a dominant mechanism of floodplain and delta-plain aggradation: Geology, v. 43, p. 875–878.

Smith, M. and S.J. Bentley Sr., 2014, Sediment capture in flood plains of the Mississippi River: A case study in Cat Island National Wildlife Refuge, Louisiana: Proceedings of the International Association of Hydrological Sciences, v. 367, p. 442.

Stone, G.W., B. Liu, D.A. Pepper, and P. Wang, 2004, The importance of extratropical and tropical cyclones on the short-term evolution of barrier islands along the northern Gulf of Mexico, USA: Marine Geology, v. 210(1), p. 63-78.

Talma, A.S., and J.C. Vogel, 1993, A simplified approach to calibrating 14C dates. Radiocarbon, v. 35, p. 317-322.

Törnqvist, T.E., J.L. González, L.A. Newsom, K. van der Borg, A.F. de Jong, and C.W. Kurnik, 2004, Deciphering Holocene sea-level history on the US Gulf Coast: A high-resolution record from the Mississippi Delta: Geological Society of America Bulletin, v. 116(7-8), p. 1026-1039.

Törnqvist, T.,E., Wallace, D. J., Storms, J. E. A., Wallinga, J., Van Dam, R.,L., Blaauw, M., . . . Snijders, E. M. A. 2008. Mississippi delta subsidence primarily caused by compaction of holocene strata. Nature Geoscience, 1(3), 173-176

Turner, R.E., 1991, Tide gauge records, water level rise, and subsidence in the northern Gulf of Mexico: Estuaries and Coasts, v. 14(2), p. 139-147.

Waelbroeck, C., L. Labeyrie, E. Michel, J.C. Duplessy, J. F. McManus, K. Lambeck, E. Balbon, and M. Labracherie, 2002, Sea-level and deep water temperature changes derived from benthic foraminifera isotopic records: Quaternary Science Reviews, v. 21, p 295-305.

Wilhite, L.P., and J.R. Toliver, 1990, Baldcypress in: silvics of North America." Volume 1, Conifers. Burns, R.M., and Honkala, B.H., tech. coords. Agriculture Handbook 654. U.S. Department of Agriculture, Forest Service, p. 563-572.

Yu, Shi-Yong, Torbjörn E. Törnqvist, Ping Hu, Quantifying Holocene lithospheric subsidence rates underneath the Mississippi Delta, In Earth and Planetary Science Letters, Volumes 331–332, 2012, Pages 21-30

Zoore, R. Z., H.J. Dowsett, S.Verardo, and T.M. Quinn, 2003, Millennial- to century-scale variability in Gulf of Mexico Holocene climate records: Paleoceanography v. 18, 1048

Appendix A. Supplementary Material

Radiocarbon dates for wood samples previously collected by scuba divers and Ben Raines at the study site.

Table A.1 Wood samples radiocarbon results

Wood Samples Radiocarbon Results							
Sample Type	**Sample #**	**Sample Name**	**$\delta^{13}C$**	**^{14}C age**	**±**	**Cal BP age**	**Cal BP range**
Wood Ben	CAMS-160062	ALAF C1	–25	51700	2600		
Wood Ben	CAMS-160064	ALAF C1 dup	–25	>52500			
Wood Ben	CAMS-160063	ALAF B1	–25	>49600			
Wood Ben	CAMS-160128	ALAF-B1 dup	–25	>51200			
Wood Diver	CAMS-167083	GOM 1A	–25	50700	3100		
Wood Diver	CAMS-167084	GOM 1B	–25	51200	3400		
Wood Diver	CAMS-167085	GOM 2A	–25	>51400			
Wood Diver	CAMS-167086	GOM 2B	–25	>52600			
Wood Diver	CAMS-167087	GOM 013A #1	–25	>48600			
Wood Diver	CAMS-167088	GOM #2	–25	52400	3900		
Wood Diver	CAMS-167089	GOM 005A	–25	>49100			

Appendix B. Frequency Contour Plots

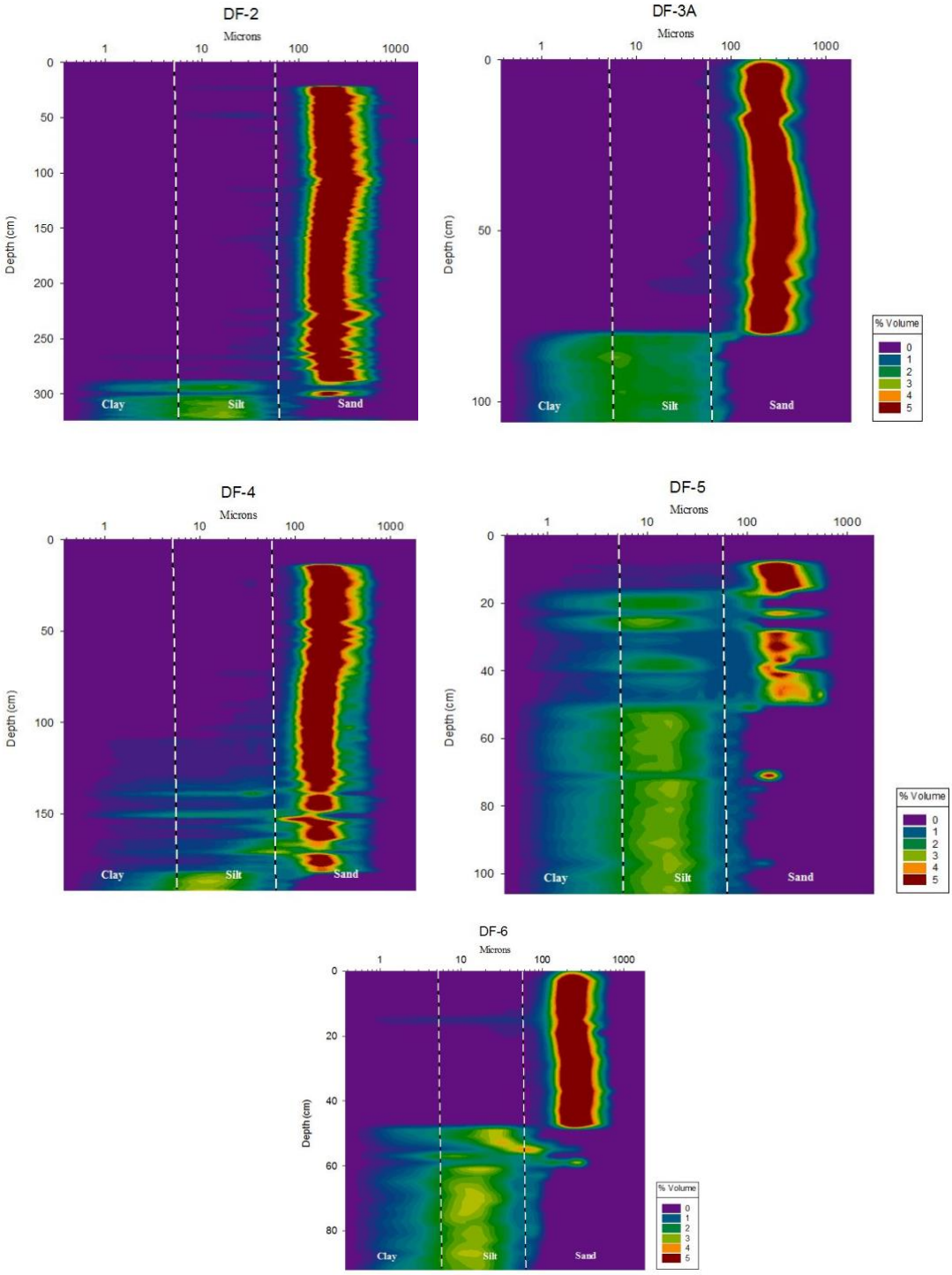

Figure B.1. Frequency contour plots for grain size distributions. Core grain size is shown as a color contour plot of % volume versus depth. Warm colors indicate dominant grain size for that depth in microns.

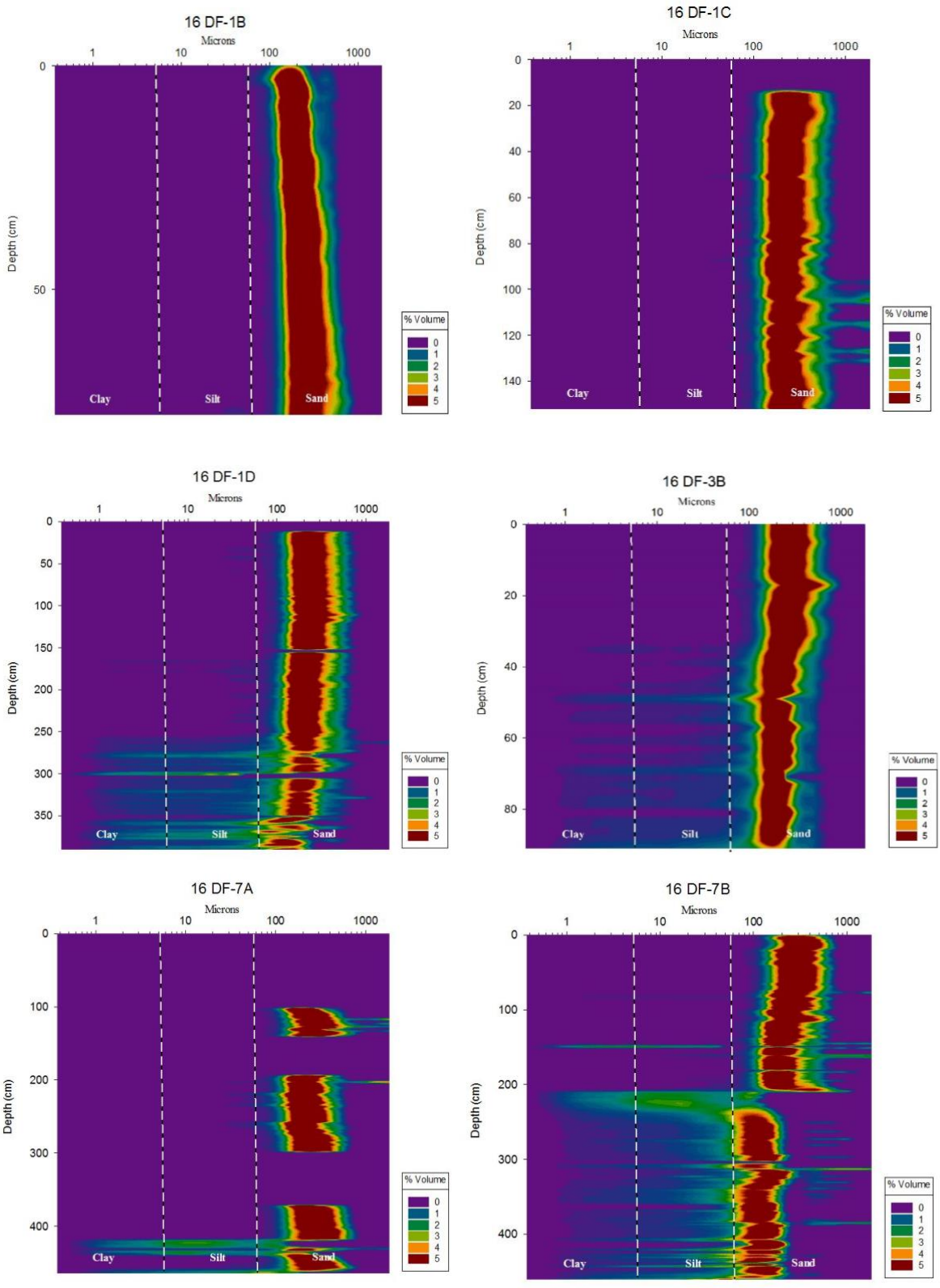
16 DF-1B
Microns
1
10
100
1000
0
50
Depth (cm)
Clay
Silt
Sand
% Volume
0
1
2
3
4
5
16 DF-1C
Microns
0
20
40
60
80
100
120
140
Depth (cm)
Clay
Silt
Sand
% Volume
16 DF-1D
Microns
0
50
100
150
200
250
300
350
Depth (cm)
Clay
Silt
Sand
% Volume
16 DF-3B
Microns
0
20
40
60
80
Depth (cm)
Clay
Silt
Sand
% Volume
16 DF-7A
Microns
0
100
200
300
400
Depth (cm)
Clay
Silt
Sand
% Volume
16 DF-7B
Microns
0
100
200
300
400
Depth (cm)
Clay
Silt
Sand
% Volume

fig. cont'd

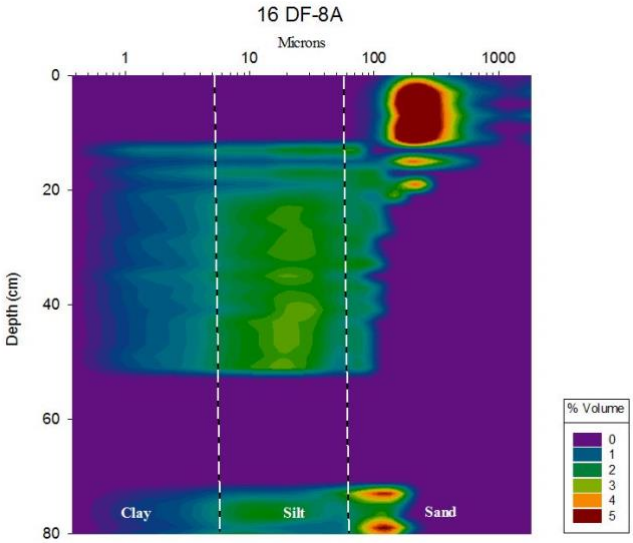
16 DF-8A
Microns
1
10
100
1000
0
20
40
60
80
Depth (cm)
Clay
Silt
Sand
% Volume
0
1
2
3
4
5

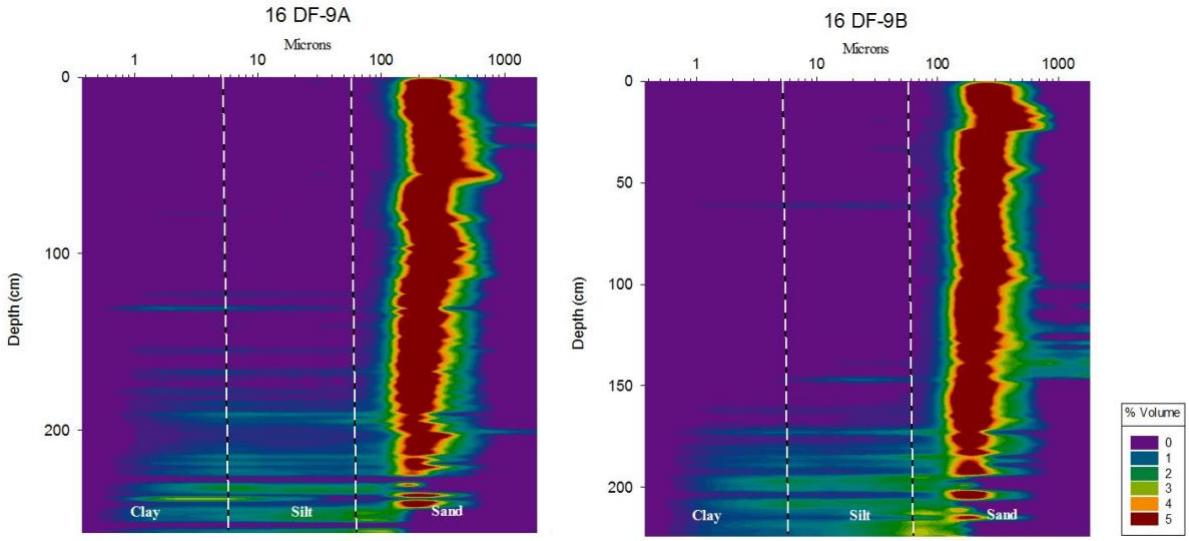
16 DF-9A
Microns
1
10
100
1000
0
100
200
Depth (cm)
Clay
Silt
Sand
16 DF-9B
Microns
1
10
100
1000
0
50
100
150
200
Depth (cm)
Clay
Silt
Sand
% Volume
0
1
2
3
4
5

Appendix C. Comprehensive Graphs

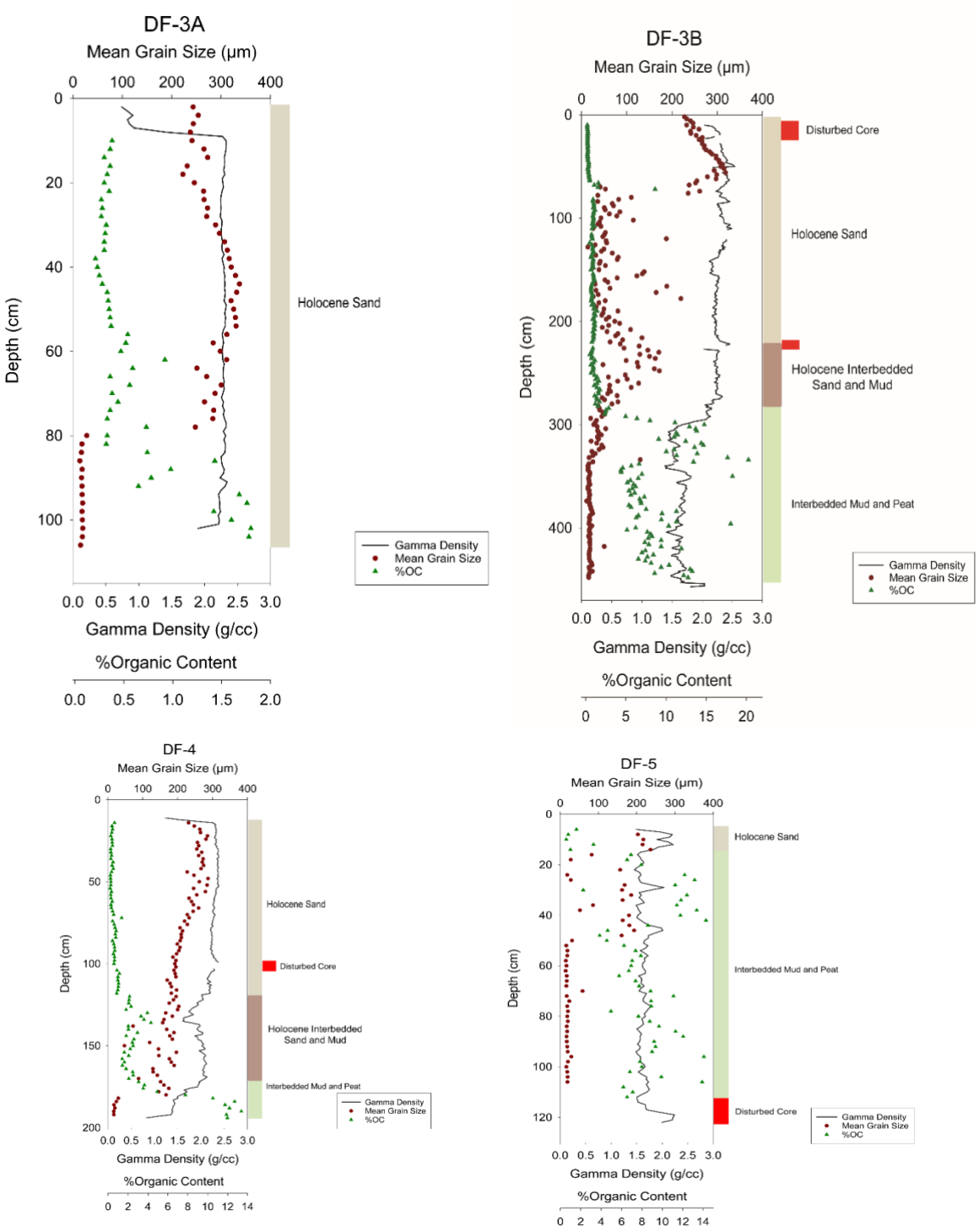

Figure C.1. Comprehensive graphs from cores collected in 2015 and 2016 showing gamma density, grain size, and organic content.

fig. cont'd

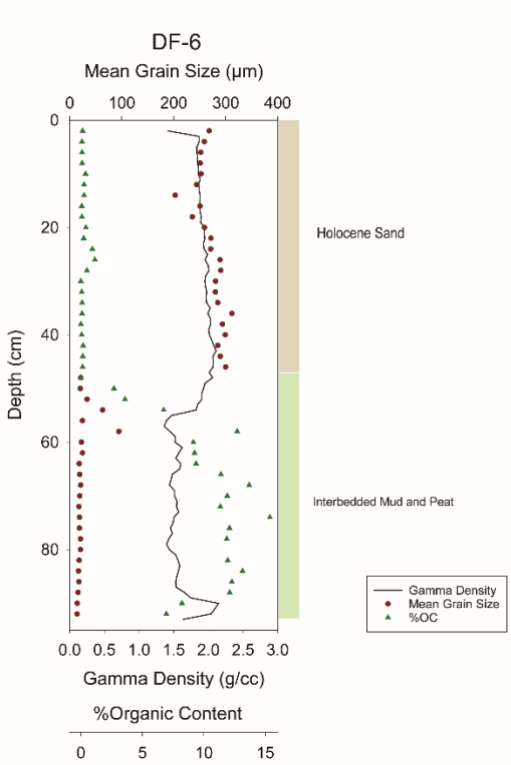
DF-6
Mean Grain Size (µm)
0 100 200 300 400
Depth (cm)
0 20 40 60 80
Holocene Sand
Interbedded Mud and Peat
Gamma Density
Mean Grain Size
%OC
0.0 0.5 1.0 1.5 2.0 2.5 3.0
Gamma Density (g/cc)
%Organic Content
0 5 10 15

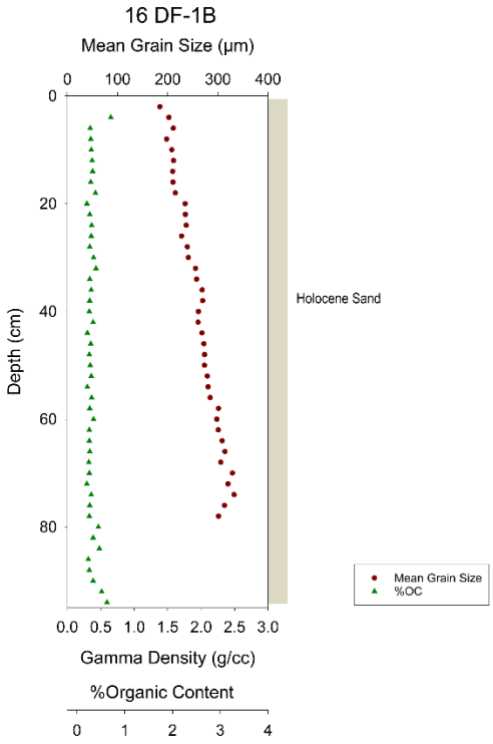
16 DF-1B
Mean Grain Size (µm)
0 100 200 300 400
Depth (cm)
0 20 40 60 80
Holocene Sand
Mean Grain Size
%OC
0.0 0.5 1.0 1.5 2.0 2.5 3.0
Gamma Density (g/cc)
%Organic Content
0 1 2 3 4

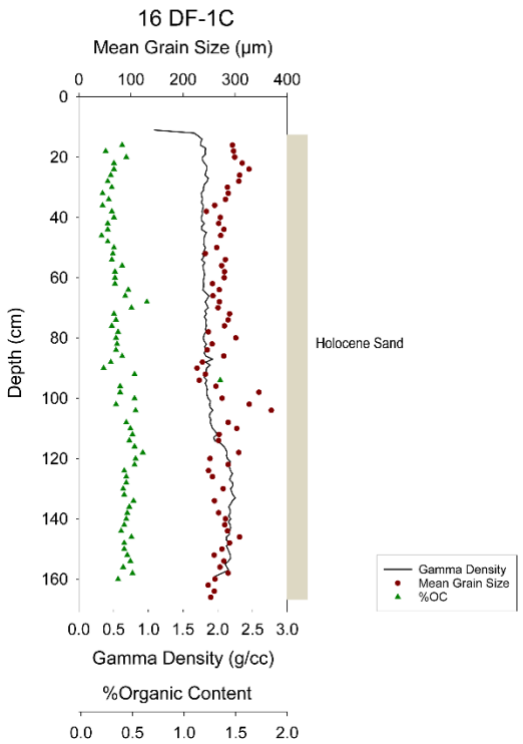
16 DF-1C
Mean Grain Size (µm)
0 100 200 300 400
Depth (cm)
0 20 40 60 80 100 120 140 160
Holocene Sand
Gamma Density
Mean Grain Size
%OC
0.0 0.5 1.0 1.5 2.0 2.5 3.0
Gamma Density (g/cc)
%Organic Content
0.0 0.5 1.0 1.5 2.0

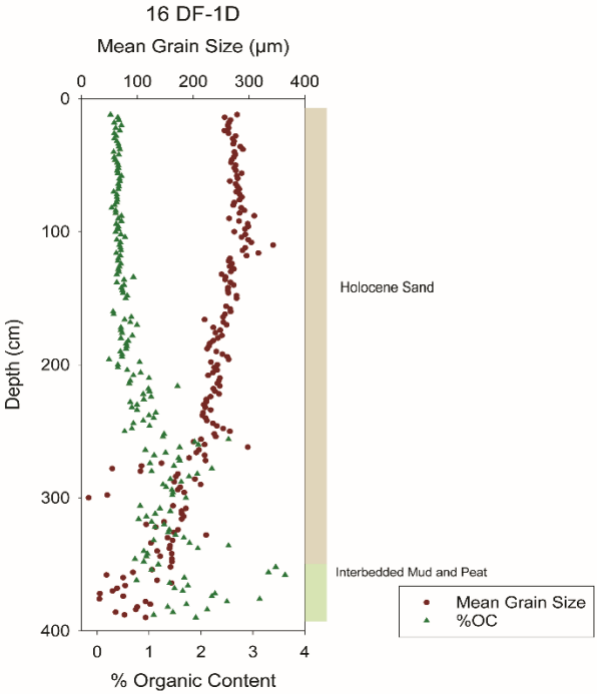
16 DF-1D
Mean Grain Size (µm)
0 100 200 300 400
Depth (cm)
0 100 200 300 400
Holocene Sand
Interbedded Mud and Peat
Mean Grain Size
%OC
0 1 2 3 4
% Organic Content

fig. cont'd

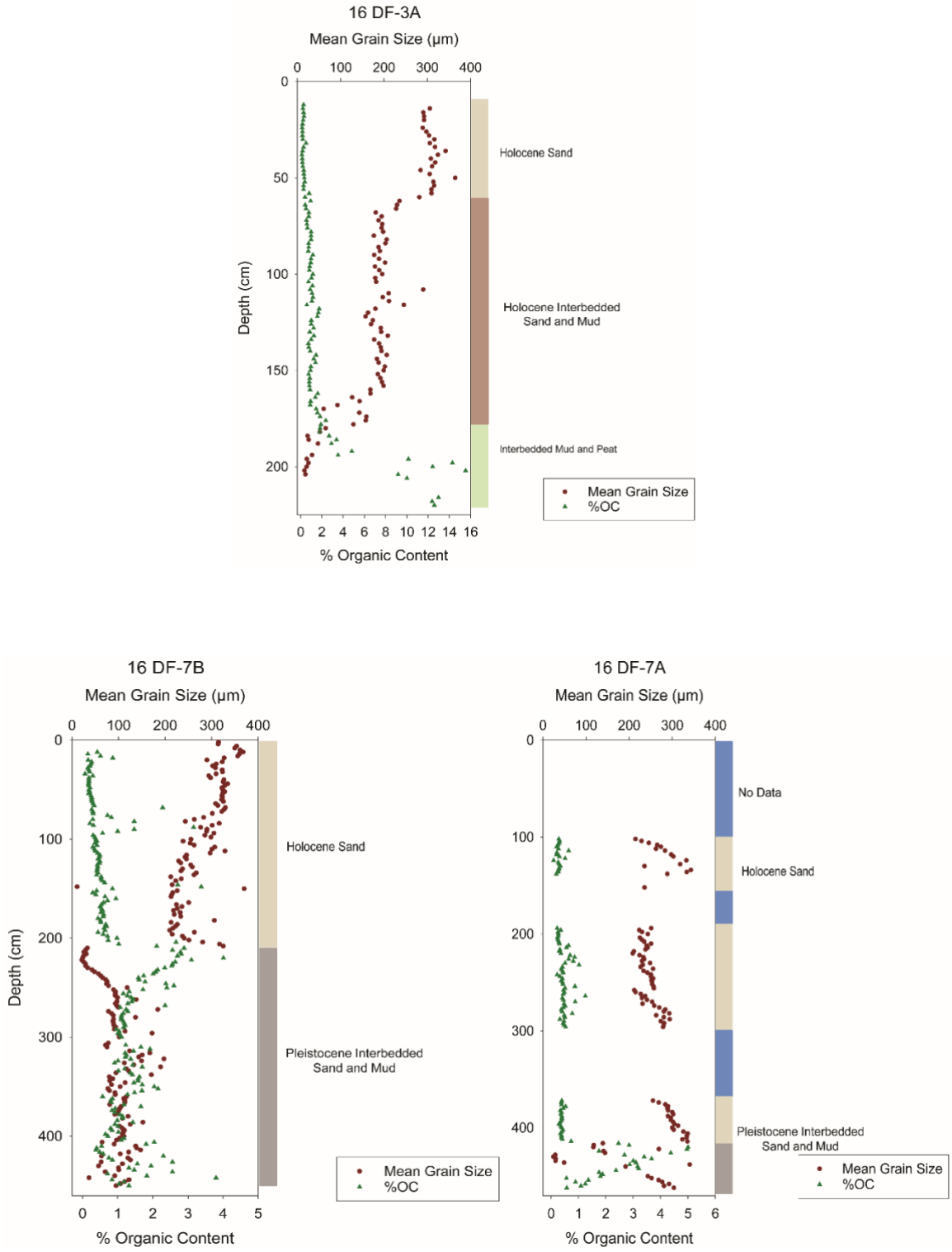
16 DF-3A
Mean Grain Size (µm)
0 100 200 300 400
Depth (cm)
0 50 100 150 200
Holocene Sand
Holocene Interbedded Sand and Mud
Interbedded Mud and Peat
Mean Grain Size
%OC
0 2 4 6 8 10 12 14 16
% Organic Content
16 DF-7B
Mean Grain Size (µm)
0 100 200 300 400
Depth (cm)
0 100 200 300 400
Holocene Sand
Pleistocene Interbedded Sand and Mud
Mean Grain Size
%OC
0 1 2 3 4 5
% Organic Content
16 DF-7A
Mean Grain Size (µm)
0 100 200 300 400
0 100 200 300 400
No Data
Holocene Sand
Pleistocene Interbedded Sand and Mud
Mean Grain Size
%OC
0 1 2 3 4 5 6
% Organic Content

fig. cont'd

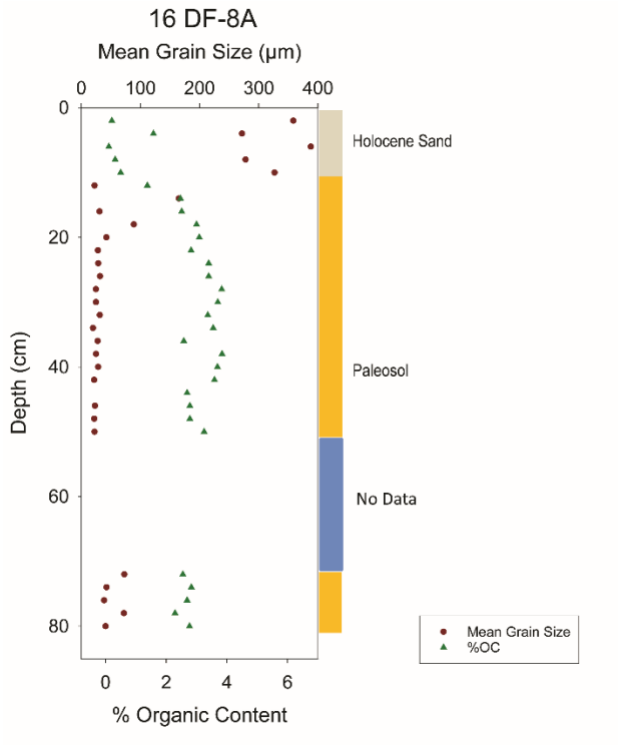
16 DF-8A
Mean Grain Size (µm)
0
100
200
300
400
0
20
40
60
80
Depth (cm)
Holocene Sand
Paleosol
No Data
Mean Grain Size
%OC
0
2
4
6
% Organic Content

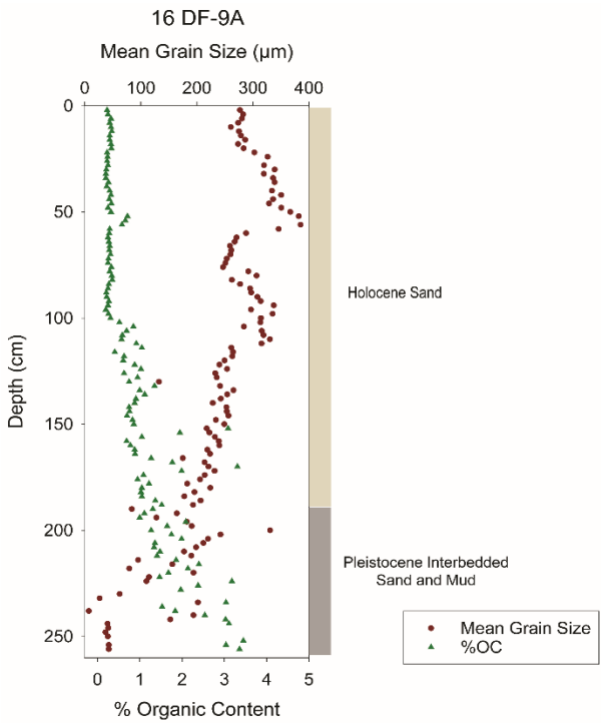
16 DF-9A
Mean Grain Size (µm)
0
100
200
300
400
0
50
100
150
200
250
Depth (cm)
Holocene Sand
Pleistocene Interbedded
Sand and Mud
Mean Grain Size
%OC
0
1
2
3
4
5
% Organic Content

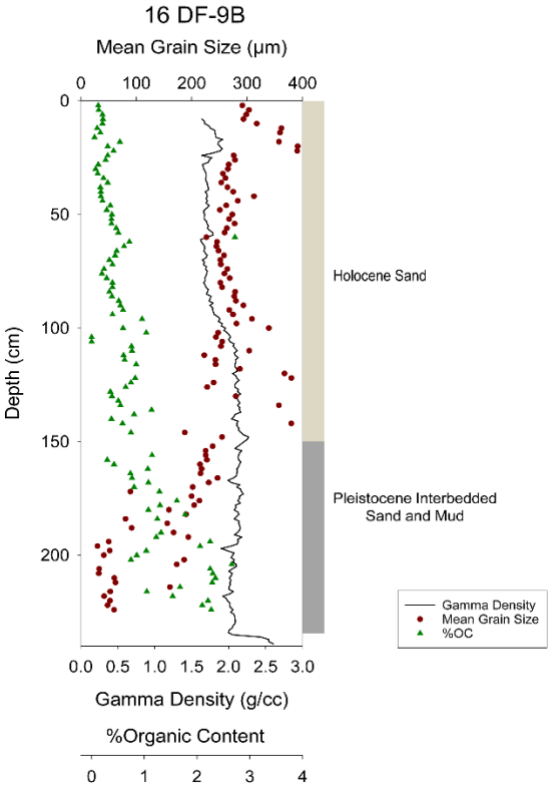
16 DF-9B
Mean Grain Size (µm)
0
100
200
300
400
0
50
100
150
200
Depth (cm)
Holocene Sand
Pleistocene Interbedded
Sand and Mud
Gamma Density
Mean Grain Size
%OC
0.0
0.5
1.0
1.5
2.0
2.5
3.0
Gamma Density (g/cc)
%Organic Content
0
1
2
3
4

Appendix D. Copyright Information

publisher's grant of permission to reprint

Suyapa M Gonzalez Rodriguez
Thu 5/10, 8:49 AM

Thank you!

James Willis <james.willis@gcags.org>
Tue 5/8, 7:48 PM
Suyapa M Gonzalez Rodriguez; james.willis@gcags.org

Reply all

Flag for follow up. Start by Thursday, May 10, 2018. Due by Thursday, May 10, 2018.

Hi Suyapa.

First congratulations on nearing the completion of your thesis--a big accomplishment.

Second this email serves that GCAGS grants to you the full authority to reproduce any and aspects, both text and illustrations, from your GCAGS publication into your LSU thesis. You can forward a copy of this email as necessary for any graduate school requirements regarding that permission.

Regards,

James Willis
GCAGS Managing Editor and Publisher


gcags.org

Facies Reconstruction of a Late Pleistocene Cypress Forest Discovered on the Northern Gulf of Mexico Continental Shelf

Suyapa Gonzalez[1], Samuel J. Bentley, Sr.[1], Kristine L. DeLong[3], Kehui Xu[2], Jeffrey Obelcz[2], Jonathan Truong[1], Grant L. Harley[4], Carl A. Reese[4], and Alicia Caporaso[5]

[1]Coastal Studies Institute and Department of Geology and Geophysics, Louisiana State University, 331 & E235 Howe-Russell Geoscience Complex, Baton Rouge, Louisiana 70803

[2]Coastal Studies Institute and Department of Oceanography and Coastal Sciences, Louisiana State University, 2165 Energy, Coast & Environment Bldg., Baton Rouge, Louisiana 70803

[3]Department of Geography and Anthropology, Louisiana State University, 227 Howe-Russell Geoscience Complex, Baton Rouge, Louisiana 70803

[4]Department of Geography and Geology, University of Southern Mississippi, 118 College Dr., Box 5051, Hattiesburg, Mississippi 39406

[5]Bureau of Ocean Energy Management, 1201 Elmwood Park Blvd., New Orleans, Louisiana 70123

GCAGS Explore & Discover Article #00196*
http://www.gcags.org/exploreanddiscover/2017/00196_gonzalez_et_al.pdf
Posted October 30, 2017.

*Article based on a full paper published in the *GCAGS Transactions* (see footnote reference below), which is available as part of the entire 2017 *GCAGS Transactions* volume via the GCAGS Bookstore at the Bureau of Economic Geology (www.beg.utexas.edu) or as an individual document via AAPG Datapages, Inc. (www.datapages.com), and delivered as an oral presentation at the 67th Annual GCAGS Convention and 64th Annual GCSSEPM Meeting in San Antonio, Texas, November 1–3, 2017.

ABSTRACT

A previously buried bald cypress forest (*Taxodium distichum*) was discovered on the continental shelf seafloor, offshore of Orange Beach, Alabama, USA, in ~20 m water depth. The forest was likely buried in the late Pleistocene, possibly exhumed by Hurricane Ivan in 2004, and is now exposed as stumps in life position. In August 2015 and July 2016, submersible vibracores and geophysical data were collected to investigate local stratigraphy and mode of forest preservation. This study focuses on analysis of the longest and most stratigraphically complete vibracore, DF–1 (4.78 m). This core revealed, from top to bottom, a surface of Holocene transgressive sands, underlain by in-

Vita

Suyapa Michell Gonzalez Rodriguez was born and raised in the exotic land of Honduras. After her junior year in high school, she studied abroad in Germany for a year where she learned her third language and traveled to many countries in Europe. She came to Baton Rouge on August 2013 to pursue her bachelors of science in geology at Louisiana State University. Following graduation, Suyapa enrolled in a master's program in geology at the same institution. Upon graduation in August 2018, she hopes to pursue a career in marine geology.